

**GENESIS OF RIFTING-RELATED BASALT MAGMA IN YAMATO
BACKARC BASIN, JAPAN SEA**

日本海・大和海盆の背弧リフト活動に伴う玄武岩質マグマの生成過程

Shigeru YAMASHITA

山下 茂

①

**GENESIS OF RIFTING-RELATED BASALT MAGMA IN
YAMATO BACKARC BASIN, JAPAN SEA**

Shigeru YAMASHITA

December, 1990

Abstract

Ocean Drilling Program Leg 127/128 cored the basement igneous bodies at the two sites in the Yamato backarc basin which now occupies southern half of the basinal area of the Japan Sea. The basement igneous bodies predominantly occur as numerous sills intruded nearly synchronously with deposition of the host marine sediments estimated at about 20 to 15 Ma. The sediments were accumulated with rapid regional submergence, suggesting that the igneous bodies were emplaced at the same time as the regional rifting.

The rifting-related igneous bodies predominantly have high-Al basalt compositions. Mass balance among the rocks and the phenocrysts suggests that, in terms of major-element chemistry, the entire rifting-related basaltic rocks were derived from the compositionally similar parent, i.e., the least differentiated aphyric sample (MgO = 10 wt.%), by crystallization differentiation. According to back-track of olivine-maximum fractionation on the least differentiated sample, the primary magma has high-Al basalt composition with MgO = 14 wt.%.

The rifting-related basaltic rocks are also characterized by low K₂O contents comparable to in MORBs, suggesting the little amounts of magmatic H₂O (< 1 wt.%). The anhydrous melting experiments on the least differentiated sample suggest that the differentiation processes, which made the entire rifting-related basaltic rocks, is likely at almost anhydrous conditions (< 1 wt.% H₂O) of relatively low pressures. It is also experimentally suggested that the least differentiated sample can not be a representative of primary magma because of lack of the liquidus orthopyroxene at varying pressures. On the other hand, synthetic of the estimated primary magma is experimentally proved to coexist with harzburgite mantle at anhydrous condition around 14 kbar (40 to 50 km below surface), 1340°C.

The rifting-related primary magma has higher TiO_2 , Al_2O_3 , and Na_2O contents, and lower FeO^*/MgO ratio and K_2O content than the temporally-associated primary magma of the Pacific coastal range, NE Japan where the lithosphere was not remarkably stretched in the period. The compositional discrepancies could not be produced by different extents of partial melting of compositionally uniform mantle peridotite. Alternatively, lower melting extent of *refractory* source mantle peridotite beneath the rift explains the compositional discrepancies except for in K_2O . The discrepancy in K_2O is probably due to differential contributions of slab-derived K^+ -bearing H_2O fluid, i.e., the *less refractory* source mantle peridotite beneath the Pacific coastal range was effectively flushed by the H_2O fluid.

Taking into account the shallow-seated top of low velocity channel (ca. 30 to 50 km) beneath the present basinal area, the rifting-related primary magma was probably produced by partial melting of the shallow-seated top of the *refractory* high-temperature mantle peridotite ("asthenosphere") itself. Beneath the Pacific coastal range, on the other hand, the *less refractory* source mantle peridotite probably uprose sporadically ("diapir") from deeper-seated high-temperature mantle in the mantle wedge because of the less frequent supply (lower average productivity of igneous materials and higher extent of melting) and the effective flushing in slab-derived H_2O fluid compared to beneath the rift. Accordingly, the deep-seated physicochemical structure beneath the rift bore extensive partial melting of the shallow-seated *refractory* high-temperature mantle (> ca. 1300°C) which was probably underlain by the *less refractory* high-temperature mantle. The partial melting is likely to have been associated with stretching or detachment of the overlying low-temperature rigid mantle.

CONTENTS

Acknowledgements -----	1
Chapter 1 Introduction -----	1
Chapter 2 Background objectives -----	4
§2-1 Geological and geophysical backgrounds-----	4
§2-2 Basement igneous bodies: rifting-related magmatism-----	12
<i>Occurrence and timing of emplacement</i> -----	12
<i>Volumetric aspect of rifting-related magmatism</i> -----	16
Chapter 3 Genesis of rifting-related basalt magma I: Petrography and whole rock major-element and nickel chemistry -----	18
§3-1 Analytical procedures-----	18
§3-2 Petrography-----	20
§3-3 Effect of alteration on whole rock chemistry-----	26
§3-4 Whole rock major-element and nickel chemistry-----	29
<i>General features</i> -----	29
<i>Differentiation processes</i> -----	37
<i>Least differentiated rock represents primary magma? Tentatively no</i> ---	40
<i>Estimation of major-element composition of parental primary magma</i> --	42
Chapter 4 Genesis of rifting-related basalt magma II: Melting phase relation -----	46
§4-1 Starting materials -----	46
§4-2 Experimental procedures and results -----	52
<i>Procedures</i> -----	52
<i>Results</i> -----	53
§4-3 Experimental constraints on differentiation processes -----	60
<i>Phase relation at elevated pressure in normative composition space</i> --	60
<i>Liquid line of descent of rifting-related basalt magma</i> -----	63
<i>Differential behavior in plagioclase fractionation and H₂O content in magma</i> -----	65

§4-4 Experimental constraints on production of parental primary magma -----68

Chapter 5 Genesis of rifting-related basalt magma III: Comparison with temporally-associated primary magmas of Pacific coastal range of NE Japan -----70

§5-1 Significance of early to middle Miocene volcanic activity on Pacific coastal range of NE Japan-----70

§5-2 Compositionally distinct primary magmas-----74

§5-3 Pressure and temperature of final equilibrium between primary magmas and mantle peridotite-----81

§5-4 Origin of compositional discrepancies of primary magmas-----83

Chapter 6 Discussion: Implication for deep-seated physicochemical structure beneath rift-----91

References-----98

Appendix-A Detailed lithostratigraphic columns of the cored basement of the Yamato basin during Ocean Drilling Program Leg 127/128-----111

Appendix-B Whole rock major- and trace-element X-ray florescences analyses on the basement basaltic rocks from the Yamato basin-----116

Acknowledgements

I would like to acknowledge my supervisor, Prof. Toshitsugu Fujii for his constructive advices and encouraging discussions throughout this study. I also wish to express my gratitude to Dr. Kensaku Tamaki who was a co-chief scientist, Ocean Drilling Program Leg 127, for his principal role to obtain the samples studied here. Dr. Ichiro Kaneoka kindly permitted me to quote his unpublished radiometric age determination. Prof. Shigeo Aramaki gave me facilities for X-ray fluorescence analyses.

Valuable suggestions and very helpful criticism given by Prof. Ikuo Kushiro, Drs. Mitsuhiro Toriumi, Susumu Nohda, Yoshiyuki Tatsumi, Masashi Tsukui, Yoshitugu Furukawa, Hikaru Iwamori, Takayuki Kaneko, and Mrs. Shin'ichi Kuramoto, Eddie Listanco, and Atsushi Yasuda are appreciated. My shipboard colleagues (namely "Igpets") during Ocean Drilling Program Leg 127, Drs. James Allan, Kathryn Stewart, and Peter Thy are thanked for very enjoyable shipboard collaboration with them, which is principal in this study.

Lastly, I would like to thank my mother, Ikuyo, and my friend, Yoshie Ogo for their continuous encouragements.

Chapter 1 Introduction

The Japan Sea is an inactive back-arc basin situated at active margin of the eastern Asian continent. It is generally understood that the basinal area of the Japan Sea was created by regional rifting at the active continental margin,

i.e., regional stretching and probable detachment of the rigid lithosphere, during early to middle Miocene (e.g., Hilde and Wageman, 1973; Kobayashi, 1983; Tamaki, 1988; Tamaki, Pisciotto, Allan et al., 1990). On the analogy of formation of other back-arc basins (e.g., Saunders et al., 1979; Weaver et al., 1979; Dick et al., 1980; Moore and Curray, 1982; Hawkins and Melchoir, 1985; Sinton and Fryer, 1987), it is believed that regional and intense basalt magmatism was associated with formation of the basinal area. However, nature of the magmatism, particularly the petrological significance had been obscure. It was principally due to that, within the basinal area, thick accumulation of the post-rifting sediments had precluded to obtain the rifting-related igneous rocks.

Recently, coring basement was directed at two sites in the Yamato backarc basin occupying southern part of the basinal area (Ocean Drilling Program Leg 127/128; Tamaki, Pisciotto, Allan et al., 1990; Ingle, Suyehiro, von Breyman et al., 1990). The coring successfully recovered basaltic rocks emplaced at the same time as the regional rifting, which now makes it possible to clarify the petrological significance of the rifting-related basalt magmatism concerning formation of the basinal area. The determination of genetic condition (pressure and temperature) and source mantle chemistry for basalt magma is a dominant objective of igneous petrology. The petrological study on the cored basaltic rocks will play an important role in characterizing the deep-seated physicochemical structure beneath the rift which should be linked with style of the formation of the basinal area.

In the past decades, the concept of backarc rifting has been established together with the deep-seated physicochemical structure behind intra-oceanic arcs (e.g., Mariana trough; Sinton and Fryer, 1987; Lau basin; Hawkins and Melchoir, 1985). The regional rifting which created basinal area of the Japan Sea presumably bear a principal distinctness from the rifting behind intra-

oceanic arcs, i.e., pre-existing thick subcontinental mantle as previously pointed out by Nohda et al. (1988). Therefore, apart from the specific geological problem surrounding the evolution of basinal area of the Japan Sea, the petrological study on the cored basaltic rocks may involve an importance to understand a role of subcontinental mantle during regional rifting at active continental margin.

This study principally contributes the basic observational information needed to construct the deep-seated physicochemical structure beneath the rift which created the Yamato backarc basin. In the following Chapter 2, spatial and temporal distribution of the basement basaltic bodies in the Yamato backarc basin is documented with respect to the magmatic activity synchronized with the regional submergence and rifting at the area. Petrographical and compositional characteristics of the rifting-related basaltic rocks are described in Chapter 3 in order to discriminate their parental primary magma. In Chapter 4, physical aspects (pressure and temperature) of genesis of the rifting-related primary magma are considered together with the differentiation character on the basis of results of the high-pressure melting experiments. In Chapter 5, genesis of the rifting-related primary magma is compared with that of the temporally-associated, but spatially distinct primary magma of the Pacific coastal range, NE Japan where considerable stretching of the lithosphere did not occur in the period (e.g., Yamaji, 1990). The obtained observational petrological information is synthesized in Chapter 6 in order to construct a possible model for the deep-seated physicochemical structure beneath the rift.

Chapter 2 Background objectives

§2-1 Geological and geophysical backgrounds

The Japan Sea is a back-arc basin lying on the active margin of the eastern Asian continent. It consists principally of basinal area with about 2.0 to 3.7 km of water depth and several high-standing blocks rising by about 2.0 km above adjacent basinal area (Fig.2-1).

It is generally understood that the basinal area was created by rifting of the active margin of the eastern Asian continent, i.e, stretch of the continental lithosphere with regional subsidence and extensive volcanism followed by sea-floor spreading (e.g., Hilde and Wageman, 1973; Ludwig et al., 1975; Kobayashi, 1983; Celaya and McCabe, 1987; Tamaki, 1985; 1988; Maruyama et al., 1989). The magnetic inclinations in the Neogene strata on the main lands of Japan show drastic change during early to middle Miocene (e.g., Otofujii et al., 1985; Tosha and Hamano, 1988). The investigators concluded that the northeastern and the southwestern Japan rotated clockwise and counter-clockwise, respectively, relative to the mainland Asia during the period. Accordingly, the present main lands of Japan are believed to have drifted trenchward during early to middle Miocene. It was probably relevant to formation of the basinal area of the Japan sea (e.g., Otofujii et al., 1985).

The high-standing blocks scattered within the basinal area (Fig.2-1) are thought to be foundered continental fragments in the formation of basinal area on the basis of the crustal velocity structure with thickness and P-wave velocity of > 20 km and 6 km/sec., respectively (Ludwig et al., 1975), and the out-cropped

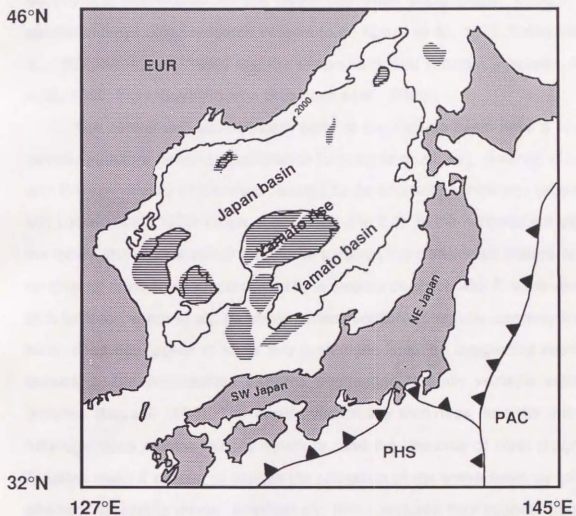


Fig.2-1. Simplified bathymetry of the present Japan Sea. Hatched areas represent foundered continental fragments according to Tamaki (1985). PAC, PHS, and EUR denote Pacific plate, Philippine Sea plate, and Eurasia plate, respectively.

granitic materials (granite and quartz diorite) showing K/Ar age up to 300 Ma (Tamaki, 1988; Kaneoka et al, 1990).

The Yamato basin is the basinal area occupying southern part of the Japan Sea (Figs.2-1 and 2-2). In this decade, large amounts of geological and geophysical information on the basin has been accumulated through the several surveys using research vessels (e.g., Honza et al., 1979; Tokuyama et al., 1987; Kobayashi, 1988) and the deep sea drilling (Tamaki, Pisciotto, Allan et al., 1990; Ingle, Suyehiro, von Breymann et al., 1990).

The central and southwestern parts of the Yamato basin have a crustal velocity structure bearing resemblance to oceanic crust, i.e., absence of layer with P-wave velocity of 6 km/sec., except for its anomalous thickness (about 15 km; Ludwig et al., 1975; Hirata et al., 1989) (Fig.2-3). In the northeastern part of the basin, the crustal velocity structure involves the transitional feature to the continental crust, that is represented by a velocity structure with P-wave velocity of 6 km/sec (Hirata et al., personal communication). Magnetic anomaly in the basin does not appear to show any systematic lineation suggesting sea-floor spreading, but complicated patterns suggesting laterally variable volcanic terranes (Isezaki, 1986). The anomalous crustal thickness, and the laterally heterogeneous crustal velocity structure, and the absence of clear magnetic lineation make it difficult to explain the formation of the entire basin by simple sea-floor spreading model. Alternatively, these features may suggest that the basin was, at least partially, created by stretching of the continental lithosphere with extensive magmatism.

The Yamato basin has flat abyssal plain punctuated sporadically by seamounts (Fig.2-2). The abyssal plain was developed by thick accumulation of marine sediments (Tokuyama et al., 1987). The underlying basement is situated

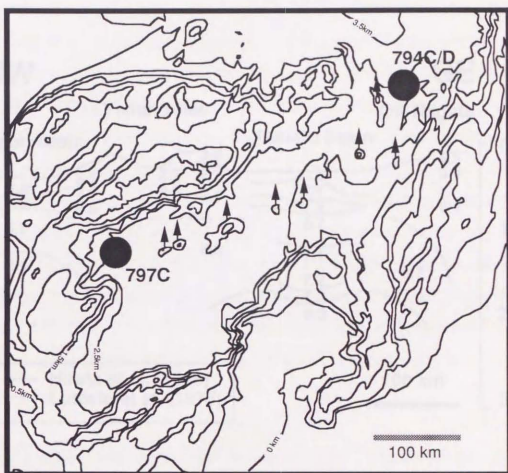


Fig.2-2. Bathymetry of the Yamato basin. Bathymetric contour interval is 0.5 km. 797C and 794C/D denote locations of the cored basement during Ocean Drilling Program Leg 127/128 (Tamaki, Pisciotto, Allan et al., 1990; Ingle, Suyehiro, von Breyman et al., 1990).

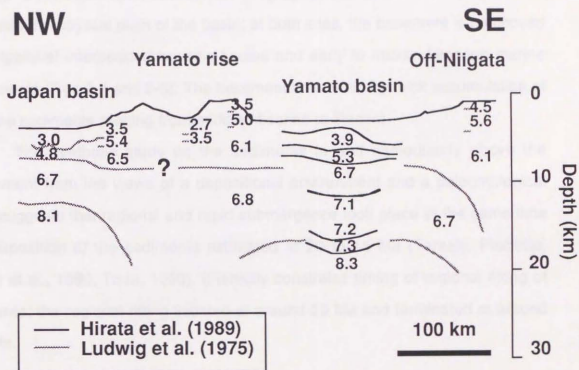


Fig.2-3. P-wave velocity structure of the crust beneath the Japan Sea along the direction of NW - SE (after Ludwig et al., 1975; Hirata et al., 1989).

at 1.0 to 2.0 km below the sea-floor (e.g., Tamaki, 1988; Hirata et al., 1989) (Fig.2-3). Coring of the basement was first attained by Ocean Drilling Program Leg 127/128 at the two sites (Hole 797C and Hole 794C/D) which are located at western margin and northeastern center of the basin, respectively (Fig.2-2) (Tamaki, Pisciotto, Allan et al., 1990; Ingle, Suyehiro, von Breyman et al., 1990). It revealed the successive stratigraphic columns until the basement beneath the abyssal plain of the basin; at both sites, the basement is composed principally of interbedded basaltic bodies and early to middle Miocene marine sediments (Figs.2-4 and 2-5). The basement is overlain by thick accumulation of marine sediments ranging from middle Miocene to Recent.

The synthetic study on the sediments in and immediately above the basement from the views of a depositional environment and a paleontological age suggests that regional and rapid submergence took place at the same time as deposition of the sediments estimated at 20 to 15 Ma (Tamaki, Pisciotto, Allan et al., 1990; Tada, 1990). It directly constrains timing of regional rifting of the area; the regional rifting initiated at around 20 Ma and terminated at around 15 Ma.

The seamounts scattering within the present Yamato basin (Fig.2-2) are considered to be volcanic edifices (e.g., Tamaki, 1988; Kaneoka et al., 1990). They rise by a few km above the adjacent basement (Tamaki, 1988). A series of dredge hauls were directed at the out-cropped tops of the seamounts (Kobayashi, 1988; Syedin, 1988; Yamashita 1988a; 1988b; Kaneoka et al., 1990). The dredged materials are dominated by mildly-alkaline intermediate volcanic rocks which are compositionally distinct from the basement basaltic bodies (Fig.2-5). Tokuyama et al. (1987) found volcanic clastic apron sediments distributed only around the seamounts using seismic reflection profiling. The

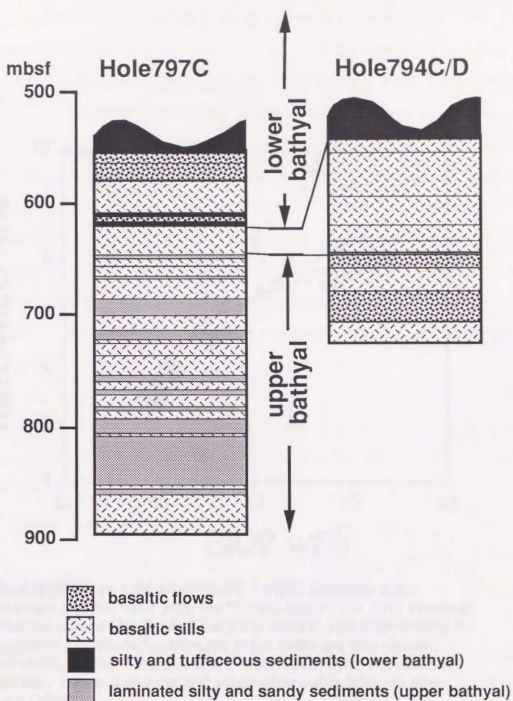


Fig.2-4. Schematic lithostratigraphic columns of the cored basement of the Yamato basin during Ocean Drilling Program Leg 127/128 (Tamaki, Pisciotto, Allan et al., 1990; Ingle, Suyehiro, von Breyman et al., 1990). Locations of each site are shown in Fig.2-2. Vertical axis represents penetrated depth below sea-floor. Note that depositional environments of the intercalated sediments change from lower bathyal to upper bathyal with penetrated depth at both sites.

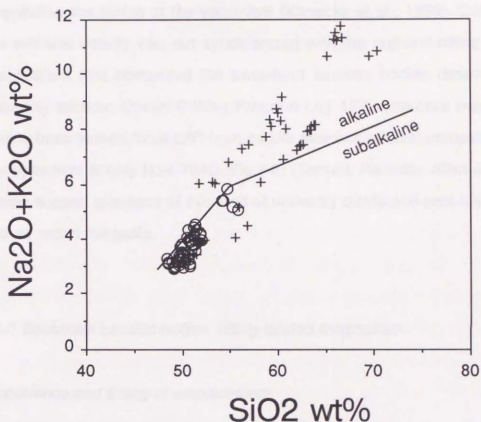


Fig.2-5. SiO₂ vs. total alkali (Na₂O + K₂O) variations of the basement basaltic rocks from the Yamato basin (O). Only unaltered rocks are plotted (§3-3). Mildly alkaline volcanic rocks comprising the sporadically distributed seamounts in the basin are also shown (+; Yamashita, 1988a; Kaneoka et al., 1990; Yamashita, unpublished). Boundary between alkaline and subalkaline suites followed after Kuno (1966).

volcanic clastic apron sediments appear to overlie the basement directly. It suggests that the volcanic activity took place just after the regional rifting and the resulted formation of the basement. The dredged intermediate volcanic rocks show $^{39}\text{Ar}/^{40}\text{Ar}$ radiometric ages ranging from 17 to 11 Ma, also suggesting this timing of the volcanism (Kaneoka et al., 1990). Consequently, the volcanic activity was not synchronized with the regional rifting, unlike the magmatism that comprised the basement basaltic bodies described in the following section. Ocean Drilling Program Leg 127 recovered many volcanic clastic beds named "blue tuff" from middle Miocene interval immediately above the basement at only Hole 794C (Fig.2-2) (Tamaki, Pisciotto, Allan et al., 1990). It may support presence of this kind of unevenly distributed post-rifting volcanic activity within the basin.

§2-2 Basement basaltic bodies: rifting-related magmatism

Occurrence and timing of emplacement

The interbedded basaltic sills and basaltic lava flows intercalating tuffaceous, silty, and sandy marine sediments of early to middle Miocene comprise the cored sequences of basement of the Yamato basin (Figs.2-4 and 2-5) (Tamaki, Pisciotto, Allan et al., 1990; Ingle, Suyehiro, von Breyman et al., 1990). The detailed lithostratigraphy is given in Appendix-A together with brief petrographic descriptions of the basaltic bodies. This kind of composition of the basement is similar to that found in other back-arc basins (e.g., Dick et al., 1980; Einsele, 1982) and is a confirmation of the prediction made by Tokuyama et al. (1987) and Hirata et al. (1989) based on the velocity structure. Resemblance in

velocity structure of the basement is recognized throughout the basin, suggesting that this kind of basement entirely spreads in the present Yamato basin (Tamaki, Pisciotta, Allan et al., 1990).

The basement basaltic bodies predominantly occur as sills rather than as lava flows (Fig.2-4). The sills are composed of massive dolerites and medium-grained basalts (Fig.2-6(A)) with chilled marginal facies which consists of finer-grained basalts having quenched texture, i.e., spherulitic morphology of the groundmass minerals. Immediately adjacent to the sills, the intercalated sediments show baked nature, i.e., hardening and color change relative to the sediments apart from the sills, which is likely due to intrusion of the sills.

The sills are interpreted to have intruded into unconsolidated sediments based on the following: Glass shards in the tuffaceous beds intercalated in the interbedded sills show both preferred orientation and plastic deformation. It suggests that collapse and compaction of the shards occurred before significant lithification of the sediments at elevated temperature, which is likely due to intrusion of the adjacent basaltic sills (Tamaki, Pisciotta, Allan et al., 1990).

The lava flows characteristically consist of brecciated fine-grained basalts (Fig.2-6(B)). The brecciated basalts are composed of zig-saw fitted monolithologic rock fragments (almost a few cm in size) with little matrix of secondary greenish clays (originally hyaloclastite?). It is probably suggestive of auto-brecciation of the basalts due to subaqueous emplacement (e.g., Fisher and Schmincke, 1984).

Accordingly, it is suggested that emplacement of the basement basaltic bodies was nearly synchronized with the deposition of the intercalated sediments estimated at 20 to 15 Ma (Tamaki, Pisciotta, Allan et al., 1990; Tada, 1990; Yamanoi, personal communication). This timing of the emplacement is supported by that radiometric ages of the basement basaltic rocks determined

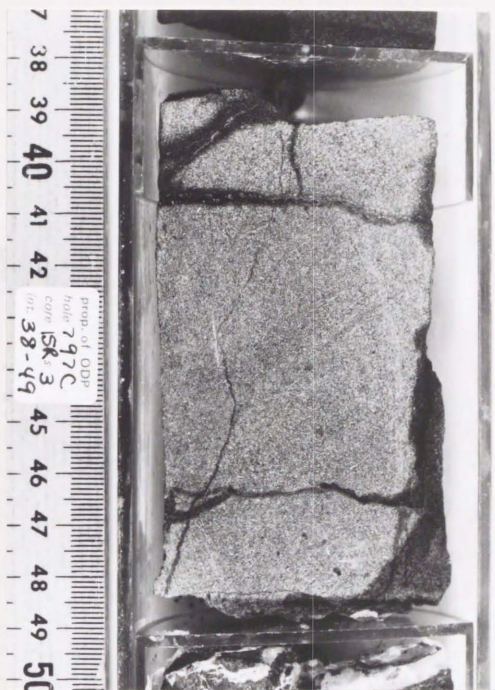


Fig.2-6(A) . Photograph of the representative massive dolerite comprising the sills of basement of the Yamato basin.

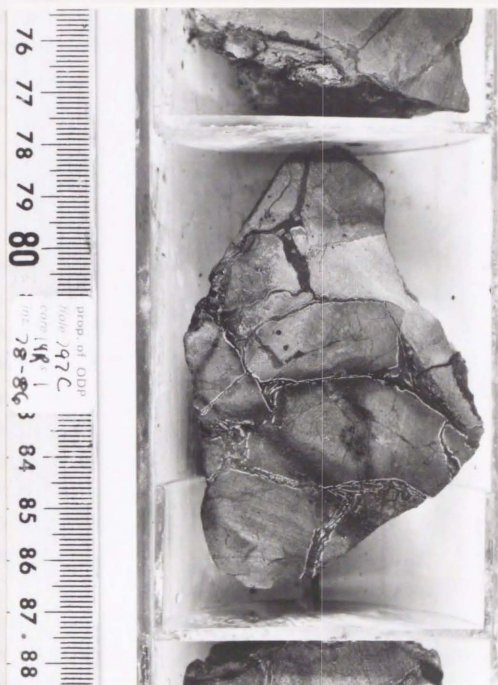


Fig.2-6(B) . Photograph of the representative auto-brecciated basalt comprising the lava flows of basement of the Yamato basin.

by $^{39}\text{Ar}/^{40}\text{Ar}$ method range from 21 to 17 Ma (Kaneoka et al., in preparation). It should be noted that, at the two sites set apart by about 300 km each other (Fig.2-2), depositional environments of the intercalated sediments change from lower bathyal to upper bathyal with penetrated depth (Tamaki, Pisciotto, Allan et al., 1990; Tada, 1990) (Fig.2-4). It suggests that the basement basaltic bodies were emplaced at the same time as the regional submergence and rifting.

Volumetric aspect of rifting-related magmatism

The abyssal plain of the present Yamato basin occupies area of about $7 \cdot 10^4 \text{ km}^2$, i.e., area approximately enclosed by contour of 2.0 km below sea-level (Fig.2-2). The actual bulk composition of crust is still unclear there because it depends on formation processes of the basin, i.e., sea-floor spreading and / or stretch of the continental lithosphere. If bulk of the crust was newly created by magmatic activity (sea-floor spreading), total volume of the igneous materials issued with the regional rifting might be close to 10^6 km^3 taking into account the crustal thickness of about 13 km without the overlying post-middle Miocene sediments. This total volume may be too large because the basin might not be totally created by sea-floor spreading as mentioned before.

Alternatively, it is assumed that at least 1 to 2 km below the surface of the basement is now composed mainly of rifting-related igneous materials. This assumption may be justified because of the following reason: Throughout the basin, the layer immediately below the surface of the basement consists of materials with P-wave velocities around 4 km/sec., whose thickness is as much as 1 to 2 km (e.g., Hirata et al, 1989; Tamaki, Pisciotto, Allan et al., 1990) (Fig.2-3). This layer corresponds to the basaltic sill/flow and sediment complex

penetrated by Ocean Drilling Program Leg 127/128. In this case, the total volume of the igneous materials issued during the regional rifting was about 0.7 to $1.4 \cdot 10^5 \text{ km}^3$.

In reality, considerable parts of the stretched continental crust might be replaced by newly created igneous materials, as seen in the rifted continental crust of the Red Sea margin (e.g., Coleman and McGuire, 1988), even if sea-floor spreading did not take part in formation of the basin. Therefore, the igneous materials of the order of 10^5 km^3 were issued during regional rifting of the area which took place for 5 m.y. (20 to 15 Ma; see §2-1).

Chapter 3 Genesis of rifting-related basalt magma I: Petrography and whole rock major-element and nickel chemistry

In this chapter, the rifting-related basaltic rocks forming the basement of the Yamato basin are petrographically characterized. Also, several aspects of the genesis of the basaltic rocks, in particular their differentiation processes and the probable major-element composition of their parental primary magma, are discussed on the basis of their petrographic features and whole rock major-element and nickel chemistry. Magmatic processes such as crystallization differentiation and partial melting are well reflected in major-element and nickel chemistry.

§3-1 Analytical procedures

The rifting-related basaltic rocks were examined with a hand lens and microscope to identify their texture, constituent phases, and extent of alteration. The chemical compositions of constituent minerals were determined with wavelength dispersive microprobe (JEOL Type 733) at Ocean Research Institute, University of Tokyo. Acceleration voltage, beam current, and beam diameter were maintained at 15 kV, 12 nA, and 2 microns, respectively, throughout the analyses. The data correction method followed after Bence and Albee (1968).

Whole rock major- and trace-element analyses were performed using X-ray fluorescence spectrometry at on-board of D/V (Drilling Vessel) *JOIDES Resolution* and at Earthquake Research Institute, University of Tokyo (ERI). The analytical method is principally same at both laboratories. Severely altered

parts, and veins and fractures filled by secondary minerals were carefully removed from the rocks before crushing. The samples were soaked in distilled water and alcohol to avoid sea water contamination, and then, powdered in tungsten-carbide mortar. The sample powders were fused in Pt-Au crucible together with lithium tetraborate flux for the major-element analyses. The trace-element analyses were made on the pressed-powder pellets. Details of the XRF analyses at *D/V JOIDES Resolution* and at ERI are given in Tamaki, Pisciotto, Allan et al. (1990) and Aramaki (1987), respectively. The loss on ignitions (LOIs) were obtained on-board *D/V JOIDES Resolution* by drying the sample powders at 110°C for 8 hours, and then by weighing them before and after heating at 1030°C in air. All data set of whole rock XRF analyses on the rifting-related basaltic rocks are given in Appendix-B.

The XRF analyses on the rifting-related basaltic rocks were initially made at *D/V JOIDES Resolution*. Several additional analyses on the microscopically unaltered basaltic rocks were performed at ERI. Accordingly, possible inter-laboratory biases in the XRF analyses were examined at ERI by analyzing the strictly same powder lots used in the on-board analyses at *D/V JOIDES Resolution* (Appendix-B). The inter-laboratory biases seem to be present in the obtained TiO_2 , FeO^* , MnO , Na_2O , K_2O , and Cr contents, but show no significant differences, i.e., well below 0.05 to 0.1 wt% for the elements, except for Na_2O (0.3 wt.%) and Cr (40 ppm). For the other elements, the differences do not exceed their analytical accuracies of each laboratories. In this study, all petrological interpretations will be done taking into account the inter-laboratory biases or the analytical accuracies (whichever greater for each elements). Therefore, it is justified to use the two data sets obtained at those two laboratories in a single petrological interpretation.

§3-2 Petrography

The rifting-related basaltic rocks have rather uniform petrographic characteristics except for modal amounts of plagioclase phenocrysts. They are divided into the following three groups based on their primary petrographic characteristics; (1) Group (A), aphyric basalt and dolerite; (2) Group (PM), moderately plagioclase-phyric basalt and dolerite; (3) Group (PH), highly plagioclase-phyric basalt and dolerite. The petrographical characteristics of each group and the chemical compositions of constituent minerals are summarized in Tables 3-1 and 3-2 respectively. This kind of poor petrographical variation, i.e., only varying amounts of the plagioclase phenocrysts, is common throughout Hole 797C and Hole 794C/D, so that the basaltic rocks are petrographically similar between the two holes apart by 300 km each other. It may suggest that, in the Yamato basin, the petrographically similar basaltic rocks are widely spread as basement.

The Groups (A), (PM), and (PH) contain euhedral to subhedral plagioclase phenocrysts (An₇₀₋₉₀) of less than 1 vol.%, 1 to 5 vol.%, and 5 to 15 vol.%, respectively. Anorthite contents of the plagioclase phenocrysts almost concentrate within 76 to 88. Euhedral to subhedral olivine phenocrysts (Fo₈₉₋₉₀) are sometimes present (<< 1 vol.%), but no pyroxene phenocrysts are found throughout the groups. Glomeroporphyritic clusters of plagioclase and olivine are rarely present. These observations may suggest that only plagioclase and olivine were the major liquidus phase in the differentiation of the basaltic rocks. Size of phenocrysts ranges from 1 mm to 10 mm in diameter. Groundmass consists of plagioclase (An₅₄₋₈₀), augite (Wo₄₁₋₄₆En₃₄₋₄₆Fs₉₋₂₂), olivine (Fo₈₂₋₈₉), Fe-Ti oxide, and subordinate amounts of mesostasis. Reddish

brown-colored Cr-spinel occasionally occurs as inclusions in olivine and plagioclase phenocrysts or as a groundmass constituent.

The groundmass shows variable textures and grain sizes depending on its occurrence. It shows intersertal and occasional spherulitic textures with constituent minerals less than 0.1 mm, i.e., fine-grained basalts, in the lava flows and in the chilled marginal part of sills. In the internal part of sills, nearly holocrystalline ophitic, subophitic, and intergranular textures are commonly developed, and the constituent minerals are up to 3 mm in maximum, i.e., dolerites and medium-grained basalts. In the dolerites, coarse-grained nature of their groundmass sometimes makes it difficult to distinguish the phenocrysts from the groundmass minerals by microscopic observation. In such rocks, identification of the phenocrysts was made according to the shape of the crystals, i.e., euhedral to subhedral.

Some rocks, particularly constituents of the marginal part of sills, were severely altered to form considerable amounts of secondary minerals (chlorite, smectite, saponite, K-rich mica, pyrite, and carbonate). The amounts of secondary minerals vary from < a few vol.% in slightly altered rocks to > 90 vol.% in very highly altered ones. The extent of alteration is also variable in a thin section size. In the highly altered rocks, mafic minerals and mesostasis are totally replaced by secondary minerals. The fractures and veins filled by secondary minerals often develop in the dolerites.

rock type	phenocrysts*(composition)/ modal amounts	groundmass
Group (A) Aphyric basalt & dolerite	Ol (Fo89-90)' << 1 vol.%, Pl (An76-80)' << 1 vol.%	Pl + Aug + Fe-Ti oxide \pm Ol \pm Mesostasis
Group (PM) Moderately plagioclase-phyric basalt & dolerite	Ol (An88-89)' << 1 vol.%, Pl (An76-82)' 1 to 5 vol.%	Pl + Aug + Fe-Ti oxide \pm Ol \pm Mesostasis
Group (PH) Highly plagioclase-phyric basalt & dolerite	Pl (An80-88)' 5 to 15 vol.%	Pl + Aug + Fe-Ti oxide \pm Ol(as pseudomorph) \pm Mesostasis

Table 3-1. Petrographical characteristics of the rifting-related basaltic rocks from the Yamato basin.
*: In the doleritic rocks, phenocrysts were identified by their shape, i.e., well developed euhedral form.

	1	2	3	4	5	6	7	8	9	10	11	12
Anal.ID	75	80	68	69	10	150	38	98	6	63	48	56
SiO ₂	48.18	48.29	53.08	48.32	47.11	47.09	51.16	52.64	47.65	47.03	53.71	51.57
TiO ₂	n.d.**	n.d.	n.d.	0.44	n.d.							
Al ₂ O ₃	32.52	32.19	28.62	32.37	32.30	32.05	29.17	28.49	33.06	33.75	27.00	30.27
FeO*	0.28	0.31	0.57	0.32	0.26	0.36	0.80	0.65	0.51	0.53	0.56	0.67
MnO	n.d.	n.d.	n.d.	n.d.	n.d.	n.d.	n.d.	n.d.	n.d.	n.d.	n.d.	n.d.
MgO	0.20	0.19	0.25	0.22	0.14	0.12	0.13	0.08	0.12	0.09	0.11	0.21
CaO	15.68	16.23	12.48	16.44	16.50	16.47	13.16	12.08	17.16	17.89	11.33	14.02
Na ₂ O	2.44	2.38	4.62	2.32	2.05	2.31	4.03	4.63	2.26	1.60	5.53	4.03
K ₂ O	n.d.	n.d.	n.d.	n.d.	n.d.	n.d.	n.d.	n.d.	n.d.	n.d.	n.d.	n.d.
Total	99.30	99.59	99.83	99.98	98.36	98.40	98.45	98.57	100.76	100.90	98.67	100.77
O number	8	8	8	8	8	8	8	8	8	8	8	8
Si	2.220	2.223	2.417	2.217	2.197	2.199	2.366	2.423	2.176	2.149	2.467	2.335
Ti	n.d.	n.d.	n.d.	n.d.	n.d.	n.d.	n.d.	n.d.	n.d.	n.d.	0.015	n.d.
Al	1.766	1.746	1.536	1.750	1.776	1.764	1.590	1.546	1.779	1.817	1.461	1.616
Fe*	0.011	0.012	0.022	0.012	0.010	0.014	0.031	0.025	0.019	0.020	0.022	0.025
Mn	n.d.	n.d.	n.d.	n.d.	n.d.	n.d.	n.d.	n.d.	n.d.	n.d.	n.d.	n.d.
Mg	0.013	0.013	0.017	0.015	0.009	0.008	0.009	0.006	0.008	0.006	0.007	0.014
Ca	0.774	0.800	0.609	0.808	0.824	0.824	0.652	0.596	0.840	0.876	0.557	0.680
Na	0.218	0.212	0.408	0.206	0.186	0.209	0.361	0.413	0.200	0.141	0.492	0.354
K	n.d.	n.d.	n.d.	n.d.	n.d.	n.d.	n.d.	n.d.	n.d.	n.d.	n.d.	n.d.
Total	5.002	5.006	5.008	5.009	5.003	5.017	5.010	5.005	5.023	5.009	5.022	5.025
An	0.780	0.791	0.600	0.797	0.816	0.798	0.644	0.593	0.808	0.861	0.531	0.658
Ab	0.220	0.209	0.400	0.203	0.184	0.202	0.356	0.407	0.192	0.139	0.469	0.342
Or	n.d.	n.d.	n.d.	n.d.	n.d.	n.d.	n.d.	n.d.	n.d.	n.d.	n.d.	n.d.

- 1: Core of plagioclase comprising glomeroporphyritic cluster with olivine in the 797C-12R-4/34-36 (Group (A)).
- 2: Core of plagioclase phenocryst in the 797C-12R-4/34-36 (Group (A)).
- 3: Core of groundmass plagioclase in the 797C-12R-4/34-36 (Group (A)).
- 4: Core of groundmass plagioclase in the 797C-12R-4/34-36 (Group (A)).
- 5: Core of plagioclase phenocryst in the 797C-24R-6/40-41(Group (PM)).
- 6: Core of plagioclase phenocryst in the 797C-24R-6/40-41(Group (PM)).
- 7: Core of groundmass plagioclase in the 797C-24R-6/40-41(Group (PM)).
- 8: Core of groundmass plagioclase in the 797C-24R-6/40-41(Group (PM)).
- 9: Core of plagioclase phenocryst in the 794C-4R-1/45-47 (Group (PH)).
- 10: Core of plagioclase phenocryst in the 794C-4R-1/45-47 (Group (PH)).
- 12: Core of groundmass plagioclase in the 794C-4R-1/45-47 (Group (PH)).
- 11: Core of groundmass plagioclase in the 794C-4R-1/45-47 (Group (PH)).

Table 3-2. Representative analyses of plagioclases in the rifting-related basaltic rocks.

*: All iron as divalent.

** : No detected.

	1	2	3	4	5	6	7	8
Anal.ID	8	48	13	24	103	122	68	125
SiO ₂	39.91	39.82	39.49	39.62	39.71	39.31	39.05	39.34
TiO ₂	**n.d.	n.d.						
Al ₂ O ₃	0.07	n.d.	0.06	0.06	n.d.	n.d.	n.d.	n.d.
FeO*	10.67	9.78	11.37	11.10	11.28	11.32	14.59	13.61
MnO	0.17	0.20	0.24	0.22	0.15	0.19	0.26	0.30
MgO	48.54	48.21	47.34	47.81	47.37	46.90	44.12	45.22
CaO	0.32	0.29	0.30	0.31	0.31	0.33	0.34	0.35
Na ₂ O	n.d.	n.d.	n.d.	n.d.	n.d.	n.d.	n.d.	n.d.
K ₂ O	n.d.	n.d.	n.d.	n.d.	n.d.	n.d.	n.d.	n.d.
Total	99.68	98.50	99.00	99.33	98.82	98.05	98.36	98.82
O number	4	4	4	4	4	4	4	4
Si	0.986	0.992	0.988	0.986	0.993	0.922	0.996	0.994
Ti	n.d.	n.d.	n.d.	n.d.	n.d.	n.d.	n.d.	n.d.
Al	0.002	n.d.	0.002	0.002	n.d.	n.d.	n.d.	n.d.
Fe*	0.220	0.204	0.238	0.231	0.236	0.239	0.311	0.288
Mn	0.004	0.004	0.005	0.005	0.003	0.004	0.006	0.006
Mg	1.787	1.790	1.765	1.774	1.766	1.764	1.678	1.704
Ca	0.008	0.008	0.008	0.008	0.008	0.009	0.009	0.010
Na	n.d.	n.d.	n.d.	n.d.	n.d.	n.d.	n.d.	n.d.
K	n.d.	n.d.	n.d.	n.d.	n.d.	n.d.	n.d.	n.d.
Total	3.007	3.002	3.009	3.010	3.006	3.010	3.000	3.002
Fe	89.0	89.8	88.1	88.5	88.2	88.1	84.4	85.6

1: Core of olivine comprising glomeroporphyritic cluster with plagioclase in the 797C-12R-4/34-36 (Group (A)).

2: Core of olivine phenocryst in the 797C-12R-4/34-36 (Group (A)).

3: Core of groundmass olivine in the 797C-12R-4/34-36 (Group (A)).

4: Core of groundmass olivine in the 797C-12R-4/34-36 (Group (A)).

5: Core of olivine phenocryst in the 797C-24R-6/40-41(Group (PM)).

6: Core of olivine phenocryst in the 797C-24R-6/40-41(Group (PM)).

7: Core of groundmass olivine in the 797C-24R-6/40-41(Group (PM)).

8: Core of groundmass olivine in the 797C-24R-6/40-41(Group (PM)).

Table 3-2. (continued). Representative analyses of olivines in the rifting-related basaltic rocks.

*: All iron as divalent.

**: No detected

	1	2	3	4	5	6
Anal.ID	64	74	147	161	8	11
SiO ₂	48.89	49.52	50.58	48.94	52.03	51.45
TiO ₂	1.63	1.30	0.91	1.67	0.53	0.66
Al ₂ O ₃	5.03	3.19	3.02	2.82	2.19	2.29
FeO*	8.02	10.39	6.60	11.81	7.45	7.50
MnO	0.17	0.23	0.14	0.39	0.20	0.19
MgO	13.24	13.30	15.38	11.96	15.81	15.02
CaO	21.42	20.34	20.89	20.18	21.54	21.24
Na ₂ O	0.48	0.60	0.39	0.60	0.33	0.32
K ₂ O	n.d.	n.d.	n.d.	n.d.	n.d.	n.d.
Total	99.20	98.87	97.90	98.35	100.09	98.68
O number	6	6	6	6	6	6
Si	1.839	1.882	1.906	1.887	1.923	1.929
Ti	0.046	0.037	0.026	0.048	0.015	0.019
Al	0.223	0.143	0.134	0.128	0.096	0.101
Fe*	0.252	0.330	0.208	0.381	0.230	0.235
Mn	0.006	0.007	0.004	0.013	0.006	0.006
Mg	0.742	0.754	0.864	0.687	0.871	0.839
Ca	0.863	0.828	0.844	0.834	0.853	0.853
Na	0.035	0.044	0.029	0.045	0.024	0.023
K	n.d.	n.d.	n.d.	n.d.	n.d.	n.d.
Total	4.016	4.026	4.014	4.023	4.018	4.006
Wo	0.465	0.433	0.440	0.438	0.436	0.442
En	0.400	0.394	0.451	0.361	0.445	0.435
Fs	0.136	0.173	0.109	0.200	0.119	0.123

1: Core of groundmass pyroxene in the 797C-12R-4/34-36 (Group (A)).

2: Core of groundmass pyroxene in the 797C-12R-4/34-36 (Group (A)).

3: Core of groundmass pyroxene in the 797C-24R-6/40-41 (Group (PM)).

4: Core of groundmass pyroxene in the 797C-24R-6/40-41 (Group (PM)).

5: Core of groundmass pyroxene in the 794C-4R-1/45-47 (Group (PH)).

6: Core of groundmass pyroxene in the 794C-4R-1/45-47 (Group (PH)).

Table 3-2. (continued) Representative analyses of pyroxenes in the rifting-related basaltic rocks.

*: All iron as divalent.

**: No detected.

§3-3 Effect of alteration on whole rock chemistry

In general, sea-floor alteration remarkably affects chemical composition of subaqueously emplaced igneous rock (e.g., Saunders and Tarney, 1984). Because the basaltic rocks sometimes underwent extensive alteration, any petrological interpretations based on their whole rock chemistry should be made very carefully. Some aspects of their chemical changes due to the alteration are described below, and then, a guideline to select the samples which keep their original magmatic compositions is provided.

The loss on ignition (LOI) of measured samples ranges from < 2 wt% in the slightly altered ones under a microscope to > 5 wt% in the very highly altered ones. The chemical change of the basaltic rocks due to the alteration is well expressed by variations in their CaO and K_2O contents and FeO^*/MgO ratio as function of LOI (Fig.3-1). At similar FeO^*/MgO ratio, the samples with higher LOIs show general enrichment in K_2O and depletion in CaO relative to those with lower LOIs. Because the same sense of correlations are recognized among the sample taken from different positions within a single intrusive or extrusive unit (Fig. 3-1), the variations are not only due to magmatic process, but also the alteration. In Fig.3-1, it should be noted that the samples with low LOIs (< 2.5 wt%) show no significant variations in K_2O and CaO contents as their FeO^*/MgO ratio changes by 0.1 whereas the samples with high LOIs (> 2.5 wt%) exhibit large and quite scattered variations at the same change of their FeO^*/MgO . It is likely, therefore, that at least the samples with low LOIs < 2.5 wt% preserve their original CaO and K_2O contents.

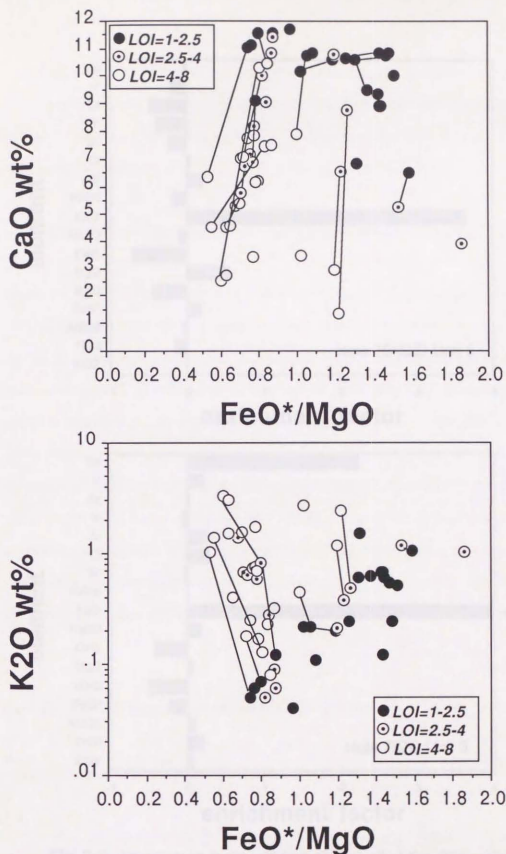


Fig.3-1. CaO, K₂O, and FeO*/MgO variations of the rifting-related basaltic rocks as a function of the amounts of loss on ignition (LOI). Analyses on the samples taken from a single intrusive or effusive unit are connected by tie-lines.

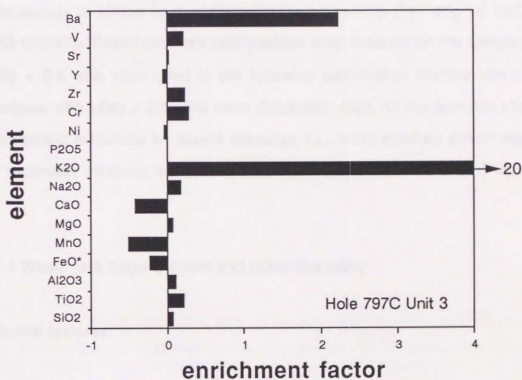
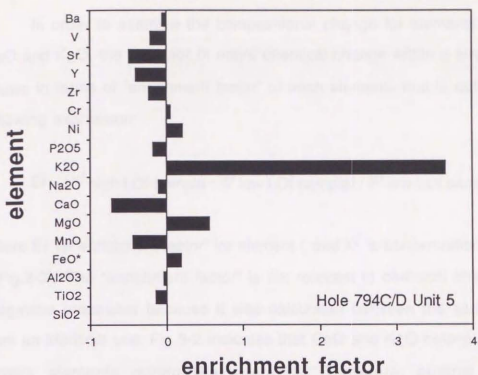


Fig.3-2. Chemical changes within a single unit of the rifting-related basaltic rocks due to alteration. The "enrichment factor" is defined in text. The elements with quite low abundances around a few ppm (see Appendix-B) are ignored because the abundances are close to their analytical errors.

In order to examine the compositional change for elements other than CaO and K₂O, the behavior of entire chemical change within a single unit are shown in terms of "enrichment factor" of each elements that is defined by the following expression:

$$E_i = (X^i_{\text{high LOI sample}} - X^i_{\text{low LOI sample}}) / X^i_{\text{low LOI sample}},$$

where E_i is "enrichment factor" for element i , and X^i is concentration of element i (Fig.3-2). The "enrichment factor" is not relevant to chemical change due to magmatic processes because it was calculated between the samples taken from an identical unit. Fig.3-2 indicates that CaO and K₂O belong to the most mobile elements during the alteration. Therefore, original magmatic composition is almost kept in the samples preserving their original CaO and K₂O contents. Based on these relationships, only analyses on the samples with LOIs < 2.5 wt% were used in the following petrological interpretations. The analyses with LOIs > 2.5 wt% were discarded. Also, all the samples showing microscopic evidences for severe alteration, i.e., mafic minerals almost replaced by secondary minerals, were discarded even if they contain LOIs < 2.5 wt.%.

§3-4 Whole rock major-element and nickel chemistry

General features

The whole rock major-element and nickel chemistry of the unaltered basaltic rocks is given in Table 3-3. The basaltic rocks show transitional affinity between alkaline and subalkaline suites in SiO₂ vs. total alkali variation (Fig.2-

HOLE	797C							
CORE	10R1/90	12R2/80	12R4/35	13R2/70	19R2/42	24R6/38	26R1/76	28R1/49
Petr.group	PM	A	A	A	PM	PM	A	A
Anal.IDs	127SB	127SB	127SB	127SB	127SB	127SB	ERI	127SB
SiO ₂	50.88	48.43	48.54	49.63	50.31	49.21	54.11	54.69
TiO ₂	1.14	0.97	0.96	1.00	0.90	0.94	3.19	2.27
Al ₂ O ₃	19.35	18.02	18.10	18.62	18.40	17.84	15.56	14.92
FeO*	6.85	7.63	7.54	7.38	6.62	7.87	11.26	9.85
MnO	0.42	0.17	0.16	0.32	0.29	0.18	0.29	0.19
MgO	6.30	9.99	10.13	7.63	8.31	8.97	5.70	6.44
CaO	11.01	11.39	11.30	11.93	11.85	11.89	4.04	5.49
Na ₂ O	3.80	3.22	3.10	3.34	3.16	2.87	4.33	4.60
K ₂ O	0.11	0.06	0.05	0.04	0.07	0.12	1.08	1.21
P ₂ O ₅	0.14	0.11	0.12	0.10	0.08	0.10	0.05	0.34
Ni	150	163	165	145	101	94	13	14
FeO*/MgO	1.09	0.76	0.74	0.97	0.80	0.88	1.98	1.53
CaO/Al ₂ O ₃	0.57	0.63	0.62	0.64	0.64	0.67	0.26	0.37

HOLE	797C	797C	797C	797C	797C	797C	794C	794C
CORE	29R1/57	29R1/69	31R2/46	31R2/36	34R1/33	45R4/15	2R1/34	2R1/77
Petr.group	A	A	A	A	A	A	PH	PH
Anal.IDs	ERI	127SB	ERI	127SB	ERI	ERI	127SB	127SB
SiO ₂	55.75	54.27	52.07	51.95	51.40	50.83	51.30	51.25
TiO ₂	1.95	2.09	1.82	1.71	2.02	1.90	1.39	1.26
Al ₂ O ₃	15.20	15.16	15.06	15.42	15.93	15.41	18.99	19.57
FeO*	9.43	9.71	10.06	9.57	9.58	10.72	8.19	8.26
MnO	0.15	0.19	0.17	0.20	0.42	0.19	0.13	0.12
MgO	5.83	6.11	6.35	6.33	6.46	7.13	5.75	5.78
CaO	6.32	6.77	10.28	10.38	9.59	10.15	9.44	9.05
Na ₂ O	3.89	4.29	3.42	3.67	3.57	2.99	3.82	3.77
K ₂ O	1.16	1.10	0.53	0.53	0.77	0.43	0.69	0.69
P ₂ O ₅	0.32	0.30	0.24	0.24	0.27	0.23	0.30	0.25
Ni	18	18	35	36	42	49	15	15
FeO*/MgO	1.62	1.59	1.58	1.51	1.48	1.50	1.43	1.43
CaO/Al ₂ O ₃	0.42	0.45	0.68	0.67	0.60	0.66	0.50	0.46

Table 3-3. Whole rock major-element and nickel chemistry of the unaltered rifting-related basaltic rocks. All the major-element compositions are recalculated to be total=100wt.%. Concentrations of major-elements and nickel are given in wt.% and ppm, respectively.

"Petr.group" denotes petrographical classification defined in §3-2.

"Anal.IDs" is explained in Appendix-B.

HOLE	794C	794C	794C	794C	794D	794D	794D	794D
CORE	3R1/115	3R1/22	4R1/42	4R2/8	1R1/96	3R3/89	12R3/36	12R3/124
Petr.group	PH	PH	PH	PH	PH	PH	A	A
Anal.IDs	ERI	127SB	127SB	ERI	128SB	128SB	128SB	ERI
SiO2	51.05	49.92	50.57	51.29	50.42	50.70	49.53	49.61
TiO2	1.31	1.13	1.08	1.25	1.30	1.29	1.66	1.67
Al2O3	19.56	20.91	19.98	19.39	19.48	18.35	16.01	16.00
FeO*	7.95	7.92	7.71	7.65	9.18	9.13	10.80	10.68
MnO	0.12	0.12	0.13	0.12	0.13	0.12	0.18	0.15
MgO	5.28	5.38	5.91	5.73	6.37	6.66	7.53	7.63
CaO	10.72	10.61	10.47	10.34	8.87	9.63	11.01	10.79
Na2O	3.14	3.29	3.35	3.22	3.44	3.29	3.03	3.08
K2O	0.66	0.54	0.59	0.74	0.61	0.63	0.12	0.19
P2O5	0.22	0.20	0.22	0.22	0.20	0.21	0.13	0.15
Ni	15	16	17	17	12	21	82	85
FeO*/MgO	1.51	1.47	1.31	1.34	1.44	1.37	1.43	1.40
CaO/Al2O3	0.55	0.51	0.52	0.53	0.46	0.53	0.68	0.67

HOLE	794D	794D	794D	794D	794D	794D	794D
CORE	13R1/81	13R1/122	14R1/81	18R1/144	19R1/11	20R1/1	20R1/20
Petr.group	A	A	A	A	A	A	A
Anal.IDs	128SB	ERI	128SB	128SB	128SB	ERI	128SB
SiO2	49.69	49.36	50.14	50.12	49.01	49.71	48.51
TiO2	1.54	1.55	1.67	1.70	1.53	1.51	1.50
Al2O3	15.36	16.26	15.40	18.07	17.51	17.05	16.92
FeO*	10.62	10.26	10.69	7.93	9.59	9.57	9.73
MnO	0.18	0.16	0.21	0.27	0.20	0.16	0.21
MgO	8.44	8.24	7.21	7.50	8.09	7.79	9.51
CaO	10.86	10.80	11.03	10.92	10.74	10.97	10.35
Na2O	2.89	2.97	3.23	3.07	2.95	2.84	2.87
K2O	0.25	0.21	0.24	0.22	0.20	0.18	0.22
P2O5	0.16	0.15	0.17	0.19	0.17	0.16	0.17
Ni	129	119	117	124	137	135	124
FeO*/MgO	1.26	1.25	1.48	1.06	1.19	1.23	1.02
CaO/Al2O3	0.71	0.66	0.72	0.60	0.61	0.64	0.61

Table 3-3 (continued).

5). They are also characterized by relatively high Al_2O_3 content (Table 3-3). These features make them to be classified into "high-Al basalt suite" defined by Kuno (1960). Their whole rock major-element and nickel compositions are graphically shown in a Harker-type diagram against their MgO contents which are good indicator of differentiation of basalt magma (Fig.3-3). Some rocks are quite primitive with MgO contents up to 10 wt % and Ni contents around 160 ppm. In terms of whole rock major-elements and Ni chemistry, the basaltic rocks show no systematic differences between Hole 797C and Hole 794C/D as well as in their petrographic characteristics (see §3-1). It is noted that, in Fig.3-3, the relatively differentiated rocks ($\text{MgO} \leq 7.5$ wt%) show quite large variations in major-element compositions, particularly in Al_2O_3 content, whereas the relatively primitive ones ($\text{MgO} > 7.5$ wt%) have rather little variations. This compositional affinity appears to correlate with their petrographic group (see §3-1) as described below, rather than their locality.

The whole rock major-element compositions of the basaltic rocks are classified based on their petrographic group (Fig.3-4). The aphyric rocks (Group (A)) have compositional range from 10 to 5.5 wt% of MgO. They define a compositional trend along which Al_2O_3 content gradually decreases and SiO_2 , TiO_2 , and FeO^* contents gradually increase with falling MgO. Their Na_2O and K_2O contents show rather little changes and rapid increases with decreasing MgO content at the $\text{MgO} > 7.5$ wt.% and ≤ 7.5 wt.% respectively. Their CaO content and $\text{CaO}/\text{Al}_2\text{O}_3$ ratio do not show remarkable changes with decreasing MgO at the $\text{MgO} > 7.5$ wt.%, but drastic decreases at the $\text{MgO} \leq 7.5$ wt.%.

On the other hand, the plagioclase-phyric rocks (Groups (PM) and (PH)) have slightly differentiated compositional range (9 to 5 wt.% of MgO) as compared to the range of the aphyric rocks. The Group (PH) has MgO-poorer

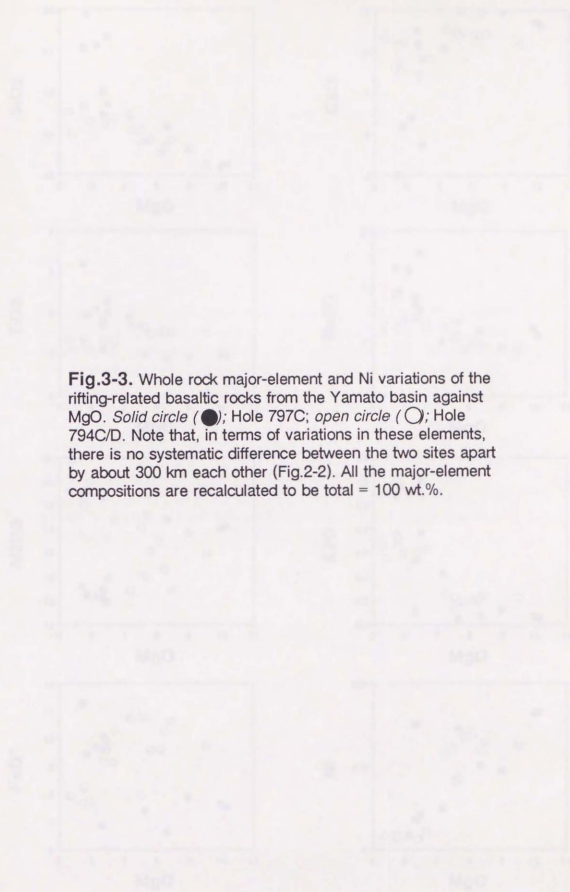


Fig.3-3. Whole rock major-element and Ni variations of the rifting-related basaltic rocks from the Yamato basin against MgO. *Solid circle (●)*; Hole 797C; *open circle (○)*; Hole 794C/D. Note that, in terms of variations in these elements, there is no systematic difference between the two sites apart by about 300 km each other (Fig.2-2). All the major-element compositions are recalculated to be total = 100 wt.%.

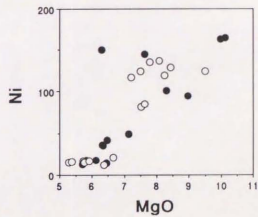
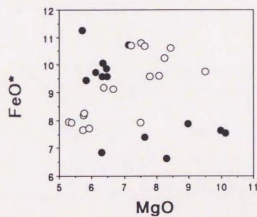
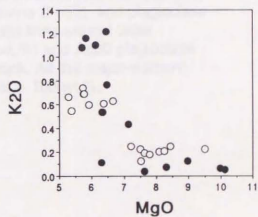
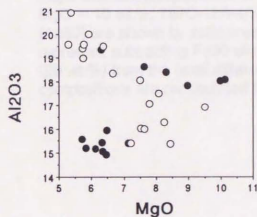
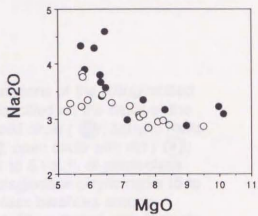
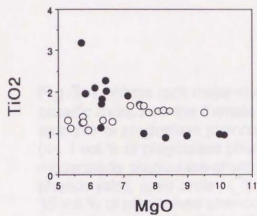
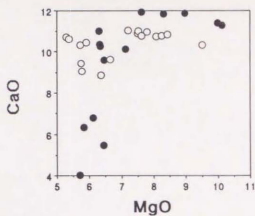
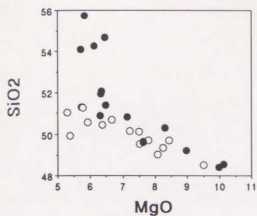
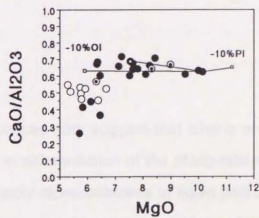
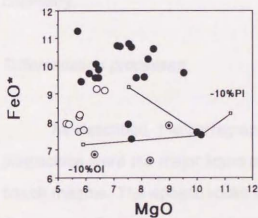
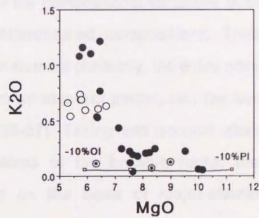
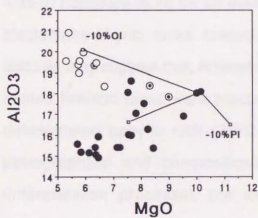
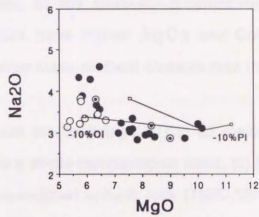
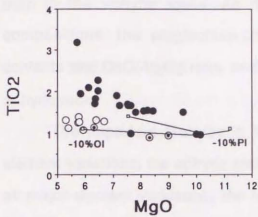
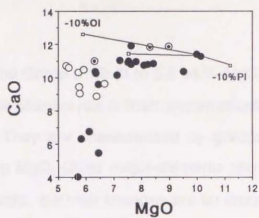
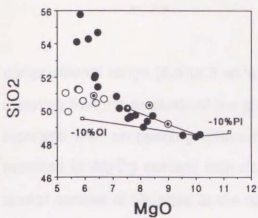


Fig.3-4. Whole rock major-element variations of the rifting-related basaltic rocks from the Yamato basin classified on the basis of the amounts of plagioclase phenocrysts. *Solid circle* (●); aphyric rocks (<< 1 vol.% of plagioclase phenocrysts); *open circle with dot* (◐); moderately plagioclase-phyric rocks (1 to 5 vol.% of plagioclase phenocrysts); *open circle* (○); highly plagioclase-phyric rocks (5 to 15 vol.% of plagioclase phenocrysts). Mass balances among major-element compositions of the least differentiated rock (aphyric; MgO = 10 wt.%; 797C-12R-4/35-37), olivine (Fo90), and plagioclase (An80) are shown by solid lines. The solid lines without letter represent subtracting Fo90 olivine (10 wt.%) and An80 plagioclase (20 wt.%) from the least differentiated rock. All the major-element compositions are recalculated to be total = 100 wt.%.



compositional range (6.5 to 5 wt.%) than the Group (PM) (9 to 6.5 wt.% MgO), meaning that the amounts of the plagioclase phenocrysts in them systematically increase with proceeding differentiation. They are characterized by gradual increase in Al_2O_3 content with decreasing MgO. Other major-elements show similar senses of changes to the aphyric rocks, but their changes are far lesser than in the aphyric rocks. As the results, at the relatively differentiated compositions, the plagioclase-phyric rocks have higher Al_2O_3 and CaO contents and CaO/ Al_2O_3 ratio, and lower other major-element contents than the aphyric rocks.

The important features in Fig.3-4 are the followings; (1) in all major-element variations, the aphyric rocks define a single compositional trend; (2) in all major-element variations, the least differentiated aphyric rock (797C-12R-4/35-37) appears to lie on an extension of the compositional variations of the plagioclase-phyric rocks toward less differentiated compositions. These features may suggest that, in terms of major-element chemistry, the entire rifting-related basaltic rocks were produced from an identical parent, i.e., the least differentiated aphyric rock (797C-12R-4/35-37). Taking into account above petrographical and compositional variations of the basaltic rocks, their differentiation processes are examined on the basis of major-element chemistry.

Differentiation processes

As described, the petrographic evidences may suggest that olivine and plagioclase were the major liquidus phase in differentiation of the rifting-related basalt magma. The aphyric rocks are probably representatives of liquid part of the magma. Providing mass balance among major-element compositions of the

aphyric rocks and the olivine and plagioclase phenocrysts (Fig.3-4), the aphyric rocks with $\text{MgO} > 7.5$ wt.% can be derived from the least differentiated aphyric rock (797C-12R-4/35-37) with $\text{MgO} = 10$ wt.% by olivine and plagioclase fractionation, approximately, in the weight ratio of 1:2.

On the other hand, the rocks with $\text{MgO} \leq 7.5$ wt.% can not be produced by olivine and plagioclase fractionation from the same parent. It is reflected in rapid decreases in CaO content and $\text{CaO}/\text{Al}_2\text{O}_3$ ratio at $\text{MgO} \leq 7.5$ wt.% (Fig.3-4). Ca-rich clinopyroxene is a secondarily crystallizing mafic mineral following olivine in common basalt magma. In general, Ca-rich clinopyroxene crystallizing from basalt magma contains moderate amounts of MgO (15 to 20 wt.%) compared to olivine. Also, Ca-rich clinopyroxene has lesser amounts of Al_2O_3 (well below 10 wt.%) and larger amounts of CaO (around 20 wt.%) as compared to plagioclase. Fractionation of mineral having this kind of compositions could result in the relatively rapid decreases in both CaO and $\text{CaO}/\text{Al}_2\text{O}_3$ with falling MgO at the MgO contents ≤ 7.5 wt.% (Fig.3-4). Therefore, it is likely that Ca-rich clinopyroxene began to crystallize at the MgO around 7 wt.% to explain major-element compositional variation of the aphyric rocks, though no Ca-rich clinopyroxene phenocryst is petrographically identified in the rocks.

The plagioclase-phyric rocks may not represent liquid part of the magma because considerable amounts of plagioclase phenocrysts occur in the rocks. The following features in Fig.3-4 should be noted:

(1) The least differentiated aphyric rock (797C-12R-4/35-37) lies on an extension of the plagioclase-phyric rocks toward less differentiated compositions in all major-element variations. The amounts of plagioclase phenocrysts increase up with falling MgO contents of the rocks, i.e.,

concentration of MgO in the rocks decreases in this order; the least differentiated aphyric rock, the plagioclase-phyric rocks of Group (PM), the plagioclase-phyric rocks of Group (PH).

(2) Discrepancy in whole rock compositions between the plagioclase-phyric rocks and the differentiated aphyric rocks appears to be larger with falling MgO.

(3) In the discrepancy, the plagioclase-phyric rocks are plotted on the "plagioclase-component" rich side of the differentiated aphyric rocks.

These observations suggest that the plagioclase-phyric rocks were produced from the least differentiated aphyric rock (797C-12R-4/35-37) without effective fractionation of crystallized plagioclase. The more differentiated plagioclase-phyric rocks with MgO \leq 7.5 wt.% show decreases in CaO and CaO/Al₂O₃ relative to both of the less differentiated plagioclase-phyric rocks with MgO > 7.5 wt.% and the least differentiated aphyric rock (797C-12R-4/35-37) (Fig.3-4). It may suggest that Ca-rich clinopyroxene fractionation contributed to create the plagioclase-phyric rocks at later stage of the differentiation, i.e., the same sense as in differentiation of the aphyric rocks.

Consequently, all the rifting-related basaltic rocks could be differentiated from an identical parent, i.e., the least differentiated aphyric rock (797C-12R-4/35-37/37). The differentiation was principally governed by olivine and plagioclase crystallization followed by Ca-rich clinopyroxene crystallization, but there were two distinct suites in the differentiation, i.e., with or without effective fractionation of the crystallized plagioclase. This point is well reflected in the differential behavior in whole rock concentrations of FeO* and Al₂O₃ against MgO between them (Fig.3-4). In the former suite, the whole rock concentration of FeO* and Al₂O₃ show strong enrichment and depletion respectively with

falling MgO, unlike in the latter suite, which are suggestive of dominance of plagioclase fractionation (e.g., Michael and Chase, 1987).

Least differentiated rock represents primary magma? Tentatively no.

The most important aspect in the petrographical and compositional features discussed above is that, at least in terms of major-element chemistry, the least differentiated aphyric rock (797C-12R-4/35-37) is probably a representative of parental magma of the entire rifting-related basaltic rocks. The 797C-12R-4/35-37 has quite primitive whole rock composition with MgO = 10 wt.%, Ni = 160 ppm, and $\text{FeO}^*/\text{MgO} = 0.75$ (Table 3-4). Its FeO^*/MgO ratio is low enough to be in equilibrium with Fo_{90} olivine assuming $\text{Fe}^{3+} / (\text{Fe}^{2+} + \text{Fe}^{3+}) = 0.1$ and $K_D = (\text{Fe}/\text{Mg})_{\text{ol}} / (\text{Fe}/\text{Mg})_{\text{liq}} = 0.3$ (e.g., Roeder and Emslie, 1970). Because the 797C-12R-4/35-37 is aphyric, the primitive nature of its whole rock composition can be recognized as that of liquid.

It is now widely accepted that basalt magma is initially created as a "primary magma" resulted from partial melting of mantle peridotite (e.g., Yoder, 1976). In the case, an exchange equilibrium should have been achieved between coexisting primary magma and mantle peridotite until the primary magma segregates from the mantle peridotite. The 797C-12R-4/35-37 might represent parental primary magma of the rifting-related basaltic rocks, if Fo_{90} olivine was common in residual mantle peridotite after the magma had segregated. However, the following facts preclude to conclude that straightforwardly: (1) Forsterite content in olivine in mantle-derived xenoliths is quite variable ($< \text{Fo}_{99}$ to Fo_{94}) depending on locality and geological setting (e.g., Maaloe and Aoki, 1977; Boyd, 1989). (2) No mantle-derived xenolith has

	797C-12R-4/35-37	Estimated parental primary magmas		
SiO ₂	48.54	47.87	48.06	47.76
TiO ₂	0.96	0.87	0.90	0.85
Al ₂ O ₃	18.10	16.39	16.88	16.06
FeO*	7.54	7.58	7.59	7.55
MnO	0.16	0.15	0.15	0.15
MgO	10.13	13.96	12.83	14.70
CaO	11.30	10.23	10.54	10.03
Na ₂ O	3.10	2.81	2.89	2.75
K ₂ O	0.05	0.05	0.05	0.05
P ₂ O ₅	0.12	0.11	0.11	0.11
NiO(ppm)	210	490	400	570
FeO*/MgO	0.74	0.54	0.59	0.51
Fo*	89.9	92	92	93
NiO*	0.23	0.41	0.36	0.46
added olvine**	0 wt.%	10 wt.%	7 wt.%	12 wt.%

Table 3-4. Chemical compositions of the least differentiated aphyric rock and the estimated parental primary magmas for it assuming back track of olvine maximum fractionation (see text).

* : Fo and NiO content in olvine in equilibrium with the above compositions.

been found in the Yamato basin, making difficult to estimate the Fo content of actual mantle olivine beneath the area.

In this study, Ni-Mg exchange partitioning between olivine and liquid was examined to discriminate parental primary magma of the rifting-related basaltic rocks of the Yamato basin. The Ni contents in mantle-derived olivines are rather constant at 0.4 ± 0.05 wt.% at various localities and geological settings whereas Fo contents in the olivines are quite variable (e.g., Sato, 1977; Elthon, 1989). The NiO content in the olivine in equilibrium with the 797C-12R-4/35-37 was calculated using experimentally obtained Ni-Mg exchange partitioning coefficient between olivine and liquid ($K_D = (\text{Ni/Mg})_{\text{ol}} / (\text{Ni/Mg})_{\text{liq}} = 2.3$; Takahashi, 1978; 1986; Kinzler et al., 1990) (Table 3-4). The calculated NiO content is only 0.23 wt.% and probably too low as a constituent of mantle peridotite. It may suggest that the 797C-12R-4/35-37 can not be a representative of the parental primary magma. It is likely that the 797C-12R-4/35-37 was differentiated from more magnesian parental primary magma.

Estimation of major-element composition of parental primary magma

The major-element composition of the parental primary magma of rifting-related basaltic rocks was estimated with the following method assuming olivine maximum fractionation: The composition of olivine which is in equilibrium with the 797C-12R-4/35-37 was calculated on the basis of Fe-Mg and Ni-Mg exchange partitioning coefficients between olivine and liquid, and then added to the rock in the weight ratio of 1:99. This step was repeated until the calculated equilibrium olivine had NiO content = 0.4 wt.% and the major-element composition of the resulted mixture was identified with that of the primary magma. The method simulates back-track of olivine maximum fractionation and

is principally same as those previously proposed by several workers (e.g., Sato, 1977; Tatsumi et al., 1983; Takahashi, 1986). Assumptions involved in this calculation are;

(1) Back-track calculation of olivine maximum fractionation can be applied. It means that only olivine was effectively fractionated to produce the 797C-12R-4/35-37 from the parental primary magma.

(2) Major element composition of olivine can be approximated by the following three components; SiO_2 , FeO , and MgO , and relative abundance of these elements obeys the stoichiometry.

(3) $\text{Fe}^{3+} / (\text{Fe}^{2+} + \text{Fe}^{3+})$ in magma is kept to be 0.1. The value is slightly higher than in mid-oceanic ridge basalts (MORBs) (e.g., Basaltic Volcanism Study Project, 1981; Michael and Chase, 1987). Basalt magma occurring at subduction zones including both volcanic arcs and back-arc basins have slightly higher $\text{Fe}^{3+} / (\text{Fe}^{2+} + \text{Fe}^{3+})$ ratios than MORBs (e.g., Gill, 1981; Hawkins and Melchior, 1985).

(4) $K_D = (\text{Fe}/\text{Mg})_{\text{Ol}} / (\text{Fe}/\text{Mg})_{\text{liq}}$ is constant at 0.3, and the pressure, temperature, and composition dependences are not significant (Roeder and Emslie, 1970; Ford et al., 1983; Takahashi and Kushiro, 1983; Ulmer, 1989).

(5) $K_D = (\text{Ni}/\text{Mg})_{\text{Ol}} / (\text{Ni}/\text{Mg})_{\text{liq}}$ is constant at 2.3, and the pressure, temperature, and composition dependences are not significant (Takahashi, 1978; 1986; Kinzler et al., 1990).

(6) NiO content in mantle olivine is 0.4 wt.%.

When about 10 wt% of olivine is added to the rock, the NiO content of calculated olivine (Fog_2) appears to be high enough to be mantle olivine. Accordingly, the 797C-12R-4/35-37 was produced by about 10 wt.% of olivine fractionation from the parental primary magma. The estimated major-element composition of parental primary magma is given in Table 3-4. The estimated parental primary

magma of rifting-related basaltic rocks has high-Al basalt composition with MgO around 14 wt.%.

The estimation was made assuming that the mantle olivine, which was finally in equilibrium with the parental primary magma, contained NiO = 0.4 wt.%. If 0.4 ± 0.05 wt.% was supposed as an uncertainty of the NiO content, the amounts of olivine added to attain the estimation would be changed, i.e., 10 ± 3 wt.% (Table 3-4). However, this kind of uncertainty does not much affect the estimated major-element composition of parental primary magma (Table 3-4).

The 797C-12R-4/35-37 contains few amounts of plagioclase and olivine phenocrysts (< 1 vol.%), suggesting that the 797C-12R-4/35-37 was saturated in plagioclase together with olivine. It may preclude to apply olivine maximum fractionation to estimate the parental primary magma composition. However, as discussed before, there is the differentiation suite in which daughter magmas were derived from the 797C-12R-4/35-37 without effective fractionation of the crystallized plagioclase. Accordingly, the few amounts of plagioclase phenocrysts in the 797C-12R-4/35-37 probably suggest that the 797C-12R-4/35-37 represents the magma which has been just saturated in plagioclase. In the case, the effect of plagioclase fractionation can be ignored to estimate the parental primary magma composition.

Alternatively, supposing that 10 wt.% of plagioclase crystallized to produce the 797C-12R-4/35-37 from the parental primary magma (the amounts are comparable to the added olivine in the estimation), the estimated major-element composition of parental primary magma would not change remarkably in terms of all major-element contents, i.e., the Al_2O_3 content increases, and MgO and FeO^* contents decrease by only about 1 wt.%, and the changes in other major-element contents is insignificant.

Consequently, as a first approximation, the estimated major-element composition of parental primary magma (Table 3-4) appears to be valid.

4-1 Clastic materials

In order to understand generation of the K2O-enriched basalt magmas in the Yandehoshan, a series of melting experiments were conducted on the following well-sorted mixture: (1) the 757C-129-405-27 sample in the usual mineralized sample matrix for melting studies, and (2) the synthesis of the estimated parental primary magmas at the K2O-enriched basaltic rocks. Chemical compositions of the starting materials are given in Table 4-1 and graphically given in the normative diagram (Fig. 4-2).

757C-129-405-27

The 757C-129-405-27 was taken from an interval just at the top of Hole 237C / Unit 3 consisting of 95% orthopyroxene (An₅₀) and clinopyroxene (Cpx₅₀) phenocrysts (see Fig. 4-1) in a matrix composed of plagioclase (An₅₀), orthopyroxene (An₅₀), Ti oxide, and subordinate minerals. Chemically, the 757C-129-405-27 is classified as a typical basalt defined by Ross (1966) and also recognized by the low K₂O content (0.21 wt%) (Table 4-1). It is a highly enriched positive -spinel with high TiO₂ (10 wt%), low FeO/TiO₂ (2.0) and high FeO/Al₂O₃ (0.8) (Table 4-1). Assuming Fe²⁺ / Fe³⁺ = 1.0 and Fe²⁺ = (Fe²⁺)_T / (Fe²⁺)_T + (Fe³⁺)_T = 0.8 (see Ross and Chatterjee, 1970; Table 4-1), the Fe²⁺ / Fe³⁺ ratio is low enough to be in equilibrium with ilmenite phenocrysts in it. It suggests, together with

Chapter 4 Genesis of rifting-related basalt magma II: Melting phase relation

§4-1 Starting materials

In order to understand generation of the rifting-related basalt magma of the Yamato basin, a series of melting experiments were directed on the following two starting materials; (1) the 797C-12R-4/35-37 which is the least differentiated sample among the rifting-related basaltic rocks cored by Ocean Drilling Program Leg 127/128, and (2) the synthetic of the estimated parental primary magma of the rifting-related basaltic rocks. Chemical compositions of the starting materials are given in Table 4-1 and graphically shown in the normative pseudoternary (Fig.4-1).

797C-12R-4/35-37

The 797C-12R-4/35-37 was taken from an internal part of basaltic sill (Hole 797C / Unit 3) consisting of little amounts of plagioclase (An_{86-90}) and olivine (Fo_{89-90}) phenocrysts ($\ll 1$ vol.%) in medium-grained intersertal groundmass of plagioclase, olivine, augite, Fe-Ti oxide, and subordinate mesostasis. Compositionally, the 797C-12R-4/35-37 is classified into high-Al basalt defined by Kuno (1960) and also characterized by quite low K_2O content (< 0.1 wt.%) (Table 4-1). It bears somewhat primitive natures with high MgO (10 wt.%), low FeO^*/MgO (0.75), and high Ni (160 ppm) (Table 4-1). Assuming $Fe^{3+} / Fe^{2+} + Fe^{3+} = 0.1$ and $K_D = (Fe/Mg)_{ol} / (Fe/Mg)_{liq} = 0.3$ (e.g., Roeder and Emslie, 1970; Takahashi and Kushiro, 1983), its FeO^*/MgO ratio is low enough to be in equilibrium with olivine phenocrysts in it. It suggests, together with

	797C-12R-4/35-37			Estimated primary magma		JB-3	
	1	2	3	4	5	6	7
SiO ₂	48.54	49.13	48.80	48.27	47.87	51.59	51.04
TiO ₂	0.96	1.05	1.00	0.93	0.87	1.45	1.45
Al ₂ O ₃	18.10	17.85	17.79	15.72	16.39	17.06	16.89
FeO*	7.54	7.85	7.33	7.66	7.58	10.27	10.69
MnO	0.16	0.14	0.15	0.14	0.15	0.17	0.16
MgO	10.13	9.68	9.21	13.79	13.96	5.32	5.20
CaO	11.30	11.29	10.97	9.67	10.23	9.91	9.86
Na ₂ O	3.10	2.81	3.03	2.59	2.81	2.98	2.82
K ₂ O	0.05	0.10	0.09	0.09	0.05	0.74	0.80
P ₂ O ₅	0.12	0.10			0.11		0.29
FeO*/MgO	0.74	0.81	0.80	0.56	0.54	1.93	2.06

Table 4-1. Chemical composition of starting materials

- 1: shipboard XRF analysis on the 797C-12R-4/35-37.
- 2: XRF analysis at ERI on the 797C-12R-4/35-37.
- 3: WDS microprobe analysis of the glass of 797C-12R-4/35-36 fused at 10kbar, 1260°C. Average of 10 analyses.
- 4: WDS microprobe analysis of the glass of synthetic of estimated primary magma fused at 15kbar, 1375°C. Average of 5 analyses.
- 5: estimated primary magma.
- 6: WDS microprobe analysis on the glass of JB-3 fused at 1atm, 1300°C, and QFM buffer. Average of 6 analyses.
- 7: recommended analysis on the JB-3 (Ando et al., 1987).

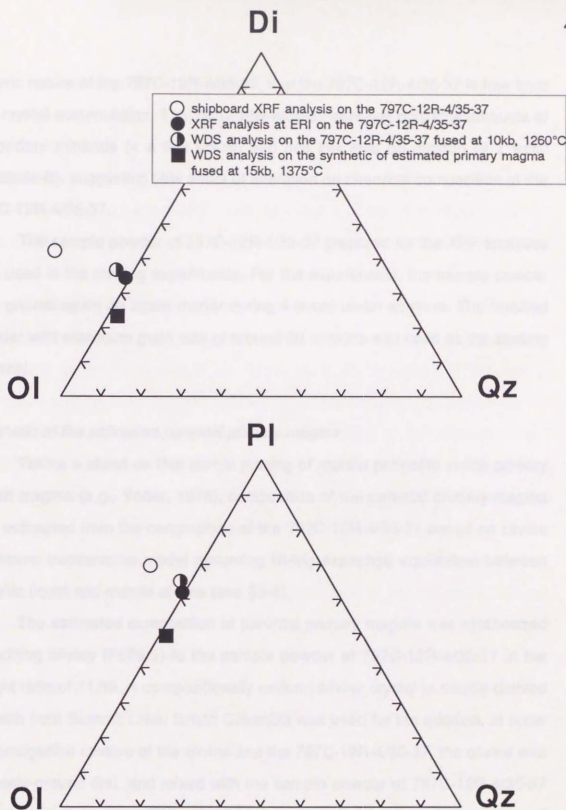


Fig.4-1. Pseudoternary projections of the starting materials. The projection method of Walker et al. (1979) was applied. It should be noted that the projection error (Elthon, 1983; Presnell and Hoover, 1984) probably contribute to displaced projections of the analyses on 797C-12R-4/35-37 made at different laboratories and by different methods. In fact, there is not severe difference among the analyses (Table 4-1).

aphyric nature of the 797C-12R-4/35-37, that the 797C-12R-4/35-37 is free from any crystal accumulation. The 797C-12R-4/35-37 contains only little amounts of secondary minerals (< a few vol.%) and has low loss on ignition (< 2 wt%; Appendix-B), suggesting little effect of alteration on chemical composition of the 797C-12R-4/35-37.

The sample powder of 797C-12R-4/35-37 prepared for the XRF analyses was used in the melting experiments. For the experiments, the sample powder was ground again in an agate mortar during 4 hours under acetone. The resulted powder with maximum grain size of around 20 microns was used as the starting material.

Synthetic of the estimated parental primary magma

Taking a stand on that partial melting of mantle peridotite yields primary basalt magma (e.g., Yoder, 1976), composition of the parental primary magma was estimated from the composition of the 797C-12R-4/35-37 based on olivine maximum fractionation model assuming Ni-Mg exchange equilibrium between basaltic liquid and mantle olivine (see §3-4).

The estimated composition of parental primary magma was synthesized by adding olivine (Fo89.5) to the sample powder of 797C-12R-4/35-37 in the weight ratio of 11:89. A compositionally uniform olivine crystal in mantle-derived xenolith from Summit Lake, British Columbia was used for the addition. In order to homogenize mixture of the olivine and the 797C-12R-4/35-37, the olivine was coarsely-ground first, and mixed with the sample powder of 797C-12R-4/35-37 in a desired proportion. This mixture was ground in an agate mortar during 4 hours under acetone. The resultant synthetic was used as the starting material. The composition was checked by analyzing the fused synthetic with a WDS

microprobe analyzer, and was proved to be identical with that of the estimated parental primary magma of rifting-related basaltic rocks (Table 4-1).

H₂O content

One of the significant compositional features of the rifting-related basaltic rocks of the Yamato basin is low K₂O contents comparable to mid-oceanic ridge basalts (MORBs) (Fig.4-2). Particularly, in the less differentiated rocks, concentration of K₂O is only 0.2 wt.% or less. Aoki et al. (1981) suggested that K₂O and H₂O contents in basalt magmas generally show good positive correlation based on analyses of the basaltic rocks produced at various geological settings involving mid-oceanic ridge. It is widely believed that MORB magmas have very low H₂O contents (Bryan and Moore, 1977; Langmuir et al., 1977; Michael and Chase, 1987). Therefore, the rifting-related basalt magma of the Yamato basin probably contains only little amount of H₂O (presumably, below 1 wt.% according to the K₂O-H₂O relation in basalt magma proposed by Aoki et al. (1981)). Such a small amounts of H₂O will not much affect melting relation of basalt system, so that the melting experiments were performed under anhydrous conditions in this study.

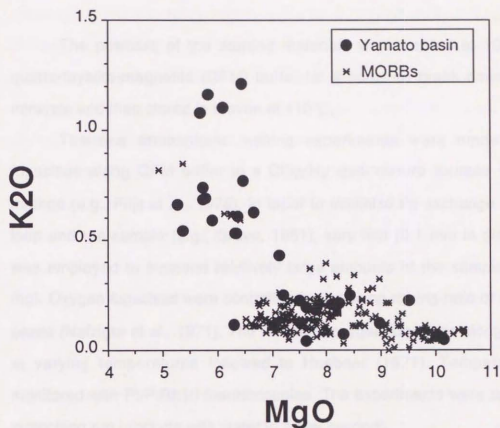


Fig.4-2. K₂O variations of the rifting-related basaltic rocks from the Yamato basin against MgO. The variation of MORB glass (Melson et al., 1977; Walker et al., 1979; O'Donnel and Presnall, 1980; Fujii and Bougault, 1983) is also shown. Note that quite low K₂O contents of the less differentiated rifting-related basaltic rocks from the Yamato basin, comparable to the MORBs.

§4-2 Experimental procedures and results

Procedures

The powders of the starting materials were heated at 1000°C under quartz-fayalite-magnetite (QFM) buffer for 8 hours to break down secondary minerals and then stored in a oven at 110°C.

The one atmosphere melting experiments were made at oxygen fugacities along QFM buffer in a CO₂/H₂ gas-mixture furnace with Pt-loop method (e.g., Fujii et al., 1978). In order to minimize Fe exchange between the loop and the sample (e.g., Grove, 1981), very thin (0.1 mm in diameter) loop was employed to suspend relatively large amounts of the sample (60 to 100 mg). Oxygen fugacities were controlled by changing mixing ratio of CO₂ and H₂ gases (Nafziger et al., 1971). The values of oxygen fugacities along QFM buffer at varying temperatures followed to Huebner (1971). Temperatures were monitored with Pt/PtRh10 thermocouples. The experiments were terminated by quenching run products with water in a few seconds.

The high-pressure melting experiments were made with a Boyd-England type solid-media apparatus of Geological institute, University of Tokyo. The hot "piston-out" method (Boyd et al., 1967) was employed. In all high-pressure runs, graphite capsules were used in the 1/2 inch-diameter furnace assemblages with Pyrex sleeves and graphite heaters. Temperatures were measured by Pt/PtRh10 thermocouples without any correction for pressure effect on thermocouple emf. In the run products, low oxygen fugacity (in wustite stability field) was probably achieved as the result of using graphite capsule (Thompson and Kushiro, 1972). The run products were quenched to temperatures below solidus in a few seconds.

The constituent phases in run products were identified with microscope and scanning electron microprobe (HITACHI Type S-530T / KEVEX energy dispersive spectrometer installed) at Earthquake Research Institute, University of Tokyo. Occasional quench crystals in the run products were discriminated on the basis of the shape, i.e., dendritic morphology. In some run products, Ca-rich clinopyroxene occur as an overgrown crystal on orthopyroxene and, rarely, olivine. Such Ca-rich clinopyroxene was interpreted to be a rapidly grown metastable phase. The chemical compositions of constituent phases were determined with a wave-length dispersive microprobe analyzer (JEOL Type 733) at Ocean Research Institute, University of Tokyo with the data correction method of Bence and Albee (1968). During the analyses, reproducibilities of the analyses were checked by analyzing the international standard basalt (JB-3) repeatedly.

Results

797C-12R-4/35-37

The run conditions and results on the 797C-12R-4/35-37 are summarized in Table 4-2 and Fig.4-3. Olivine and plagioclase nearly simultaneously crystallize as liquidus phase and are followed by Ca-rich clinopyroxene at pressures below 12 kbar to 1 atm. At pressures above 12 kbar, Ca-rich clinopyroxene appears as liquidus phase instead of olivine and plagioclase. Clinopyroxene is followed by plagioclase and olivine with descending temperature. Based on the results, the 797C-12R-4/35-37 is multiply saturated in olivine, plagioclase, and Ca-rich clinopyroxene at about 12

kbar and 1250°C. No Ca-poor pyroxene field could be found near liquidus temperatures. It is noted that plagioclase crystallizes together with olivine as the liquidus phase. This is principally due to high Al_2O_3 contents (18 wt.%; Table 4-1) and consequently due to high normative PI content in the starting basalt (Fig.4-1). In general sense, the obtained melting phase relation is consistent with the dry melting relations of some high-Al basalts previously obtained by Thompson (1974a) and Baker and Egglar (1983).

Synthetic of the estimated parental primary magma

The run conditions and results on the synthetic are summarized in Table 4-3 and Fig.4-4. At pressures below 14 kbar, olivine is the liquidus phase. Olivine is replaced by orthopyroxene at pressures above 14 kbar. The orthopyroxene is followed by Ca-rich clinopyroxene and plagioclase with descending temperature. At around 14 kbar, both olivine and orthopyroxene crystallize within 20°C below the probable liquidus temperature (1340°C), indicating that the synthetic can coexist with olivine and orthopyroxene at dry condition of around 14 kbar and 1340°C. The obtained melting relation appears to be likely for this kind of quite magnesian basalt (e.g., Green et al., 1979).

The representative compositions of minerals and glass in the run products are given in Table 4-4. The liquidus Ca-rich clinopyroxenes at high-pressures characteristically show subcalcic and aluminous nature. It is consistent with the high-pressure melting experiments of Thompson (1974b) in which crystallized Ca-rich clinopyroxenes were subcalcic augite in a wide range of starting compositions involving high-Al basalt.

Run#	Pressure(kbar)	Temperature(°C)	Duration(min)	Products
2008	10	1260	120	Liq**
2009	10	1240	120	Liq + Ol + Pl
2010	10	1220	120	Liq + Ol + Pl + Cpx
2011	11.5	1240	120	Liq + Ol + Pl + Cpx
2012	11.5	1220	120	Liq + Ol + Pl + Cpx
2013	12	1250	300	Liq + Ol + Pl
2017	12.5	1250	165	Liq + Ol + Pl + Cpx
2019	13	1300	120	Liq
2020	13	1280	105	Liq
2007	13	1280	110	Liq + Cpx
2018	13	1270	130	Liq + Cpx + Pl
2016	13	1260	210	Liq + Ol + Pl + Cpx
2006	13	1260	45	Liq + Ol + Pl + Cpx
2015	13	1250	210	Liq + Ol + Pl + Cpx
2023	13	1220	96	Liq + Ol + Pl + Cpx
2022	15	1320	70	Liq
2005	15	1300	90	Liq + Cpx
2021	15	1280	120	Liq + Cpx + Pl*(rare)
2024	15	1220	140	Liq + Ol + Pl + Cpx
AP-7	1atm	1245	10hr	Liq
AP-3	1atm	1229	19hr	Liq + Ol + Pl
AP-6	1atm	1214	16hr	Liq + Ol + Pl
AP-1	1atm	1200	36hr	Liq + Ol + Pl
AP-4	1atm	1183	51hr	Liq + Ol + Pl
AP-5	1atm	1166	56hr	Liq + Ol + Pl + Cpx

Figure 2. Melting phase relations of the 797C12R-4/35-37 low heat saturated granite melt during decompression. Melting relations of the 797C12R-4/35-37 granite melt under dry conditions.

Table 4-2. Run conditions and results of melting experiment on the 797C12R-4/35-37 at dry conditions.

Liq**: occurs as glass in run products.

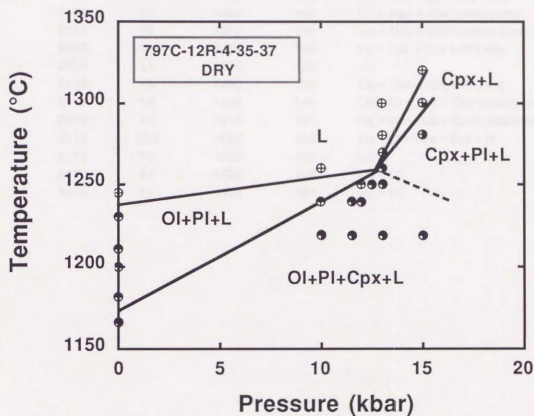


Fig.4-3. Melting phase relation of the 797C-12R-4/35-37 (the least differentiated aphyric rock among rifting-related basaltic rocks of the Yamato basin) under dry conditions.

Run#	Pressure(kbar)	Temperature(°C)	Duration(min)	Products
2103	20	1450	100	Liq**
2104	20	1422	100	Liq + Opx + Cpx*(very rare)
2101	20	1400	110	Liq + Opx + Cpx*(metastable)
2107	18	1375	120	Liq + Opx + Cpx*(quench x'stal)
2109	17	1325	130	Liq + Opx + Cpx + Pl*(rare)
2105	15	1375	120	Liq
2108	15	1300	120	Liq + Opx + Cpx + Pl*(rare)
2118	14	1330	100	Liq + Ol + Opx + Cpx*(metastable)
2112	14	1310	120	Liq + Ol + Opx + Cpx*(metastable)
2113	13.5	1280	120	Liq + Ol + Opx + Cpx + Pl
2121	13	1355	100	Liq
2110	11	1300	100	Liq + Ol
2115	11	1250	120	Liq + Ol

Fig. 4-3. Stability phase relation of the synthetic of estimated primary magma at the whole-rock results from run 2103. The synthetic was produced by using 11 wt% of silica (Pala II) in the 70TC-129-4-20-27.

Table 4-3. Run conditions and results of melting experiment on the synthetic of estimated primary magma.

Liq**: occurs as glass in run products.

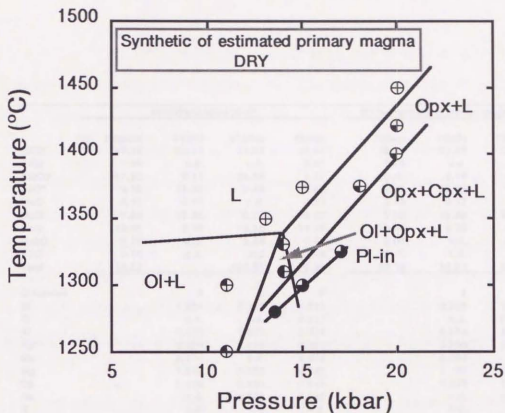


Fig.4-4. Melting phase relation of the synthetic of estimated primary magma of the rifting-related basaltic rocks under dry condition. The synthetic was produced by adding 11 wt.% of olivine (Fo89.5) to the 797C-12R-4-35-37.

	#2017(797C-12R-435-37)				#2118 (Synthetic of primary magma)		
	35/glass	41/oliv	47/plag	46/cpx	7/glass	14/oliv	12/opx
SiO ₂	47.18	39.12	51.95	49.81	48.11	39.32	55.77
TiO ₂	1.39	n.d.	n.d.	0.61	1.20	n.d.	0.14
Al ₂ O ₃	17.83	0.11	28.56	8.77	18.87	0.13	3.34
FeO*	9.78	15.32	1.48	7.29	8.00	12.29	6.63
MnO	0.11	0.17	n.d.	0.21	0.18	0.17	n.d.
MgO	7.63	42.95	0.77	18.15	9.03	45.82	31.09
CaO	10.02	0.35	14.16	13.95	10.06	0.30	2.32
Na ₂ O	3.78	n.d.	3.89	0.57	3.61	n.d.	0.12
K ₂ O	0.10	n.d.	n.d.	n.d.	0.10	n.d.	n.d.
Total	98.02		100.81	99.36	99.16	98.03	99.41
O number		4	8	6		4	6
Si		1.004	2.369	1.813		0.996	1.943
Ti		n.d.	n.d.	0.017		n.d.	0.004
Al		0.003	1.531	0.376		0.004	0.137
Fe*		0.329	0.056	0.222		0.260	0.193
Mn		0.004	n.d.	0.006		0.004	n.d.
Mg		1.643	0.052	0.985		1.730	1.614
Ca		0.010	0.690	0.544		0.008	0.087
Na		n.d.	0.343	0.040		n.d.	0.008
K		n.d.	n.d.	n.d.		n.d.	n.d.
Total		2.993	5.035	4.003		3.002	3.986
Mg/Mg + Fe*	0.588	0.833		0.816	0.668	0.869	0.893
Wo				31.08			4.57
En				56.24			85.23
Fs				12.68			10.20

Table 4-4. Representative analyses of constituent phases in the run products at high-pressures.
 *: All iron as divalent.

§4-3 Experimental constraints on differentiation processes

Phase relation at elevated pressure in normative composition space

The 797C-12R-4/35-37 is multiply saturated in olivine, plagioclase, and Ca-rich clinopyroxene at anhydrous condition around 12 kbar.(Fig.4-3). There is no Ca-poor pyroxene field near the liquidus temperatures. With these characteristics, a probable anhydrous liquidus phase boundary at around 12 kbar was constructed on plagioclase-saturated surface in the Di-Ol-Pl-Qz pseudoquaternary (Fig.4-5). Compositions of coexisting phases at temperature just below the multiple saturation point was measured in preliminary sense (Table 4-4; Run# 2017). The residual liquid coexisting with olivine + plagioclase + Ca-rich clinopyroxene at about 12 kbar is strongly depleted in Qz component as compared to the starting composition in the Ol-Di-Qz pseudoternary (Fig.4-5(A)).

It may suggest that the thermal divide on the olivine-plagioclase-Ca-rich clinopyroxene cotectic line is placed at some composition less depleted in Qz component than the 797C-12R-4/35-37 at anhydrous condition around 12 kbar. Otherwise, the residual liquid composition may be a suggestive of peritectic saturation of Ca-poor pyroxene at anhydrous condition around 12 kbar (Fig.4-5(B)). Though it is impossible to say whether the thermal divide or the peritectic relation is likely, the residual liquid coexisting with olivine + plagioclase + Ca-rich clinopyroxene will be driven toward Qz component-deficient compositions in both cases with falling temperature at around 12 kbar. This kind of topography of the anhydrous liquidus phase relation on plagioclase-saturated surface was previously suggested by several workers at pressures above 8 kbar in a wide range of starting compositions (Fig.4-5(C); high-Al basalts and

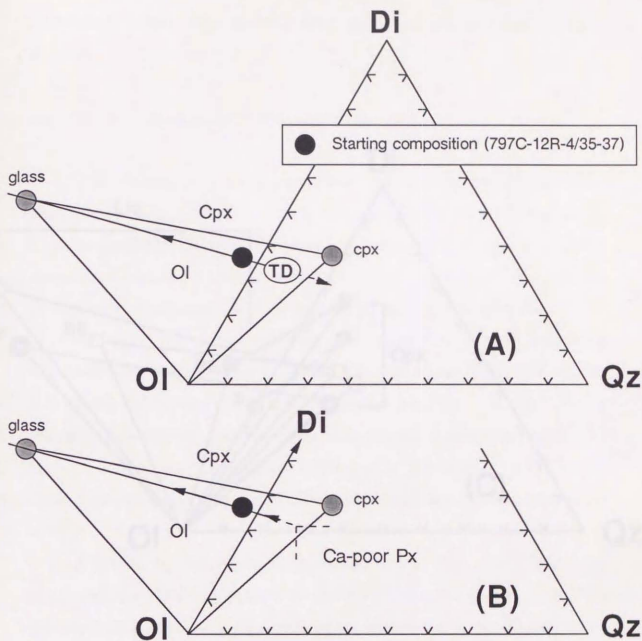


Fig.4-5. (A) and (B); Two possible phase relations of the 797C-12R-4/35-37 at 12.5 kbar. (A) denotes the thermal divide on Ol+Pl+Cpx cotectic. (B) shows the peritectic relation with Ca-poor pyroxene. The residual liquid (Run# 2017) is saturated in olivine + plagioclase + clinopyroxene and projected from Pl-component onto Di-Ol-Qz pseudoternary. (C); Comparison with previous works at elevated pressures in a wide range of starting compositions (G: MORB at 8 kbar; Grove et al., 1990; BE: high-Al basalts at 8 kbar; Baker and Eggler, 1987; S: MORB encapsulated by olivine and orthopyroxene at 10 kbar; Stolper, 1980; Y: this study at 12.5 kbar) The projection method followed after Walker et al. (1979).

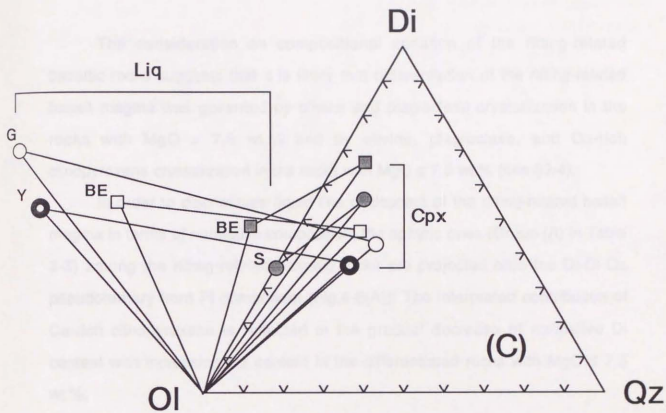


Fig.4-5. (continued)

MORBs with varying Mg#; Stolper, 1980; Baker and Egger, 1987; Grove et al., 1990).

Liquid line of descent of rifting-related basalt magma

The consideration on compositional variation of the rifting-related basaltic rocks suggests that it is likely that differentiation of the rifting-related basalt magma was governed by olivine and plagioclase crystallization in the rocks with MgO > 7.5 wt.% and by olivine, plagioclase, and Ca-rich clinopyroxene crystallization in the rocks with MgO \leq 7.5 wt.% (see §3-4).

In order to discriminate liquid line of descent of the rifting-related basalt magma in terms of normative composition, the aphyric ones (Group (A) in Table 3-3) among the rifting-related basaltic rocks are projected onto the Di-Ol-Qz pseudoternary from Pl component (Fig.4-6(A)). The interpreted contribution of Ca-rich clinopyroxene is reflected in the gradual decrease of normative Di content with increasing Qz content in the differentiated rocks with MgO \leq 7.5 wt.%.

It should be noted that, in Fig.4-6(A), some differentiated rocks are strongly enriched in Qz component as compared to the less differentiated rocks with MgO > 7.5 wt.%. Taking into account the experimentally constructed phase relations on plagioclase-saturated surface, at elevated pressures above 8 kbar, Qz-enrichment in the differentiated rocks with MgO \leq 7.5 wt.% can not be produced by crystallization differentiation of the magma compositionally similar to the less differentiated rocks such as the 797C-12R-4/35-37. At elevated pressures, the residual liquid intersects with the olivine + plagioclase + Ca-rich clinopyroxene cotectic which drives the liquid toward Qz-undersaturated compositions (Fig.4-6(A)). Walker et al. (1979) experimentally showed that the

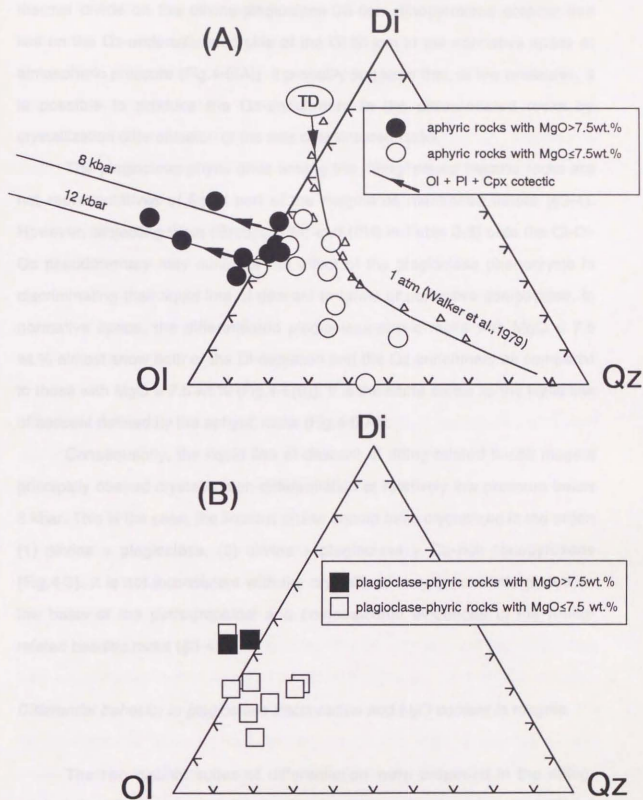


Fig. 4-6. Normative compositions of the aphyric rocks (A) and the plagioclase-phyric rocks (B). Projection method is the same as in Fig. 4-5. The olivine + plagioclase + clinopyroxene cotectic at 1 atm and the termal divide on it (Walker et al., 1979) are also shown.

thermal divide on the olivine-plagioclase-Ca-rich clinopyroxene cotectic line lies on the Qz-undersaturated side of the Ol-Di join in the normative space at atmospheric pressure (Fig.4-6(A)). It probably suggests that, at low pressures, it is possible to produce the Qz-enrichment in the differentiated rocks by crystallization differentiation of the less differentiated rocks.

The plagioclase-phyric ones among the rifting-related basaltic rocks are not representatives of liquid part of the magma as mentioned before (§3-4). However, projecting them (Groups (PM) and (PH) in Table 3-3) onto the Ol-Di-Qz pseudoternary may minimize the effect of the plagioclase phenocrysts in discriminating their liquid line of descent in terms of normative composition. In normative space, the differentiated plagioclase-phyric rocks with MgO \leq 7.5 wt.% almost show both of the Di-depletion and the Qz-enrichment as compared to those with MgO > 7.5 wt.% (Fig.4-6(B)). It is the same sense as the liquid line of descent defined by the aphyric rocks (Fig.4-6(A)).

Consequently, the liquid line of descent of rifting-related basalt magma principally obeyed crystallization differentiation at relatively low pressure below 8 kbar. This is the case, the liquidus phase should have crystallized in the order; (1) olivine + plagioclase, (2) olivine + plagioclase + Ca-rich clinopyroxene (Fig.4-3). It is not inconsistent with the crystallization sequence interpreted on the basis of the petrographical and compositional evidences in the rifting-related basaltic rocks (§3-4).

Differential behavior in plagioclase fractionation and H₂O content in magma

The two distinct suites of differentiation were proposed in the rifting-related basalt magma on the basis of petrographical and compositional evidences, i.e., with effective fractionation of the crystallized plagioclase and

without it throughout the differentiation (see §3-4). In both suites, the crystallized mafic minerals appear to have been nearly totally fractionated.

The 797C-12R-4/35-37 represents the least differentiated liquid among the observed variation of rifting-related basalt magma (see §3-4). The density-pressure relation of the 797C-12R-4/35-37 near the liquidus temperature (1250°C) was estimated using the method of Bottinga and Weill (1970) with adjustment of the effect of pressure and H₂O on density (Kushiro, 1987) (Fig.4-7). The density of calcic plagioclase, which commonly occurs as phenocryst in the rocks, is also shown in Fig.4-7.

As is clear in Fig.4-7, there are several intersections between the density curves of the 797C-12R-4/35-37 and the plagioclase, depending on the concentration of H₂O in the 797C-12R-4/35-37. It suggests that the plagioclase crystallized at the initial stage of differentiation might not be fractionated effectively and suspends in the residual liquid if both of the pressure condition and the H₂O content are suitable. For example, at anhydrous condition, the estimated density of the 797C-12R-4/35-37 appears to be comparable to that of the plagioclase at pressures around 2 kbar, so that the crystallized plagioclase would not be fractionated if the differentiation took place at anhydrous condition around 2 kbar. The critical pressure is raised to above 8 kbar if the 797C-12R-4/35-37 contains 1 wt.% of H₂O.

Around the critical pressures, only little difference in pressure condition can result in the two distinct suites of differentiation; with and without effective fractionation of the crystallized plagioclase. Taking into account the differentiation at relatively low pressure (below 8 kbar) suggested above, presence of the two distinct suites of differentiation is likely for little amounts of H₂O (below 1 wt.%) in the less differentiated magma such as the 797C-12R-

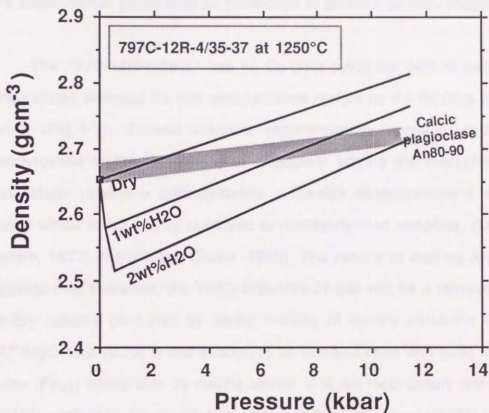


Fig. 4-7. Density-pressure relation of the 797C-12R-4/35-37 at near liquidus temperature (1250°C). The density was calculated by the method of Bottinga and Weill (1970) assuming $Fe^{3+} / Fe^{2+} + Fe^{3+} = 0.1$, and with adjustment of the effects of pressure and H₂O (Kushiro, 1987). Partial molar volume of H₂O followed after Burnham and Davis (1969). Density-pressure relation of plagioclase followed after Kushiro (1980).

4/35-37. It is not inconsistent with quite low K_2O content in the less differentiated rocks, which is a suggestive of low H_2O content in the magma.

§4-4 Experimental constraints on production of parental primary magma

The 797C-12R-4/35-37 has no Ca-poor pyroxene field at near liquidus temperatures whereas Ca-rich clinopyroxene occurs as the liquidus phase with olivine (Fig.4-3). Several workers experimentally revealed that Ca-rich clinopyroxene is the first phase to disappear among the lherzolitic mineral assemblage (olivine + orthopyroxene + Ca-rich clinopyroxene + aluminous phase) which is commonly observed in mantle-derived xenoliths. (Mysen and Kushiro, 1977; Jaques and Green, 1980). The results of melting experiments suggests that, therefore, the 797C-12R-4/35-37 can not be a representative of primary magma produced by partial melting of mantle peridotite though its FeO^*/MgO ratio (0.75) is low enough to be in equilibrium with quite magnesian olivine (FO_{90}) acceptable as mantle olivine. It is not inconsistent with relatively low NiO content in the equilibrium olivine (0.23 wt.%, i.e., probably too low as mantle olivine) calculated on the basis of Ni-Mg exchange partitioning between olivine and liquid (see §3-4).

On the other hand, the synthetic of the estimated parental primary magma can coexist with olivine and orthopyroxene at around 14 kbar, 1340°C (Fig.4-4). It suggests that the estimated parental primary magma can be produced by partial melting of mantle peridotite, supporting the estimation made by back track calculation of olivine maximum fractionation. In the case, the parental primary magma might be finally in equilibrium with harzburgitic mineral assemblage at around 14 kbar, 1340°C.

If the parental primary magma contained considerable amounts of H_2O , pressure and temperature of the equilibrium with harzburgitic mineral assemblage would be higher and lower, respectively (e.g., Tatsumi et al., 1983). Here, it is emphasized again that the less differentiated rifting-related basalt magma probably contained only little amounts of H_2O (probably below 1 wt.%) according to the quite low K_2O content and the presence of the differentiation suite without effective plagioclase fractionation. It suggests that the parental primary magma also contained only little amounts of H_2O below 1 wt.%. Tatsumi et al. (1983) conducted H_2O -deficient high-pressure melting experiments on primitive basalt compositions. Their results suggest that the effect of H_2O on melting phase relation of basalt system is not significant when H_2O content in the system does not exceed 1 wt.%.

Consequently, it is likely that the parental primary magma was finally in equilibrium with harzburgite mantle at around 14 kbar (40 to 50 km below surface), 1340°C, and then segregated.

Chapter 5 Genesis of rifting-related basalt magma III: Comparison with temporally-associated primary magmas of Pacific coastal range of NE Japan

§5-1 Significance of early to middle Miocene volcanic activity on Pacific coastal range of NE Japan

Early to middle Miocene volcanic centers are widely distributed on the present NE Japan (Fig.5-1) (Sugimura et al., 1963; Konda, 1974; Tsunakawa et al., 1983; Shuto et al., 1988; Ohguchi et al., 1989; Tsuchiya, 1989; Uto et al., 1989). On the Pacific coastal range of the NE Japan, the early to middle Miocene volcanic centers define trenchward limit of the volcanic activity at active margin of the eastern Asian continent during the period (e.g., Niitsuma et al., 1988; Tatsumi et al., 1988; Ohguchi et al., 1989). Compared with the rifting-related volcanism of the Yamato basin, the early to middle Miocene volcanic activity on the Pacific coastal range bears the following significance:

(1) According to Yamaji and Sato (1989) and Yamaji (1990), the Pacific coastal range has not undergone significant submergence during early to middle Miocene whereas other part of the present NE Japan submerged until lower bathyal as well as basinal area of the Japan Sea (Fig.5-2). It suggests that, during the period, the volcanic activity on the Pacific coastal range occurred at the area without considerable stretching of the lithosphere, unlike those in the present intra- and back-arc areas involving the Yamato basin.

(2) About 10^5 km³ of igneous materials were issued on the NE Japan (ca. 10^5 km²) during the early Neogene period older than the end of deposition of the Nishikurosawa formation (10 m.y. older than ca. 14 Ma) (Sugimura et al.,

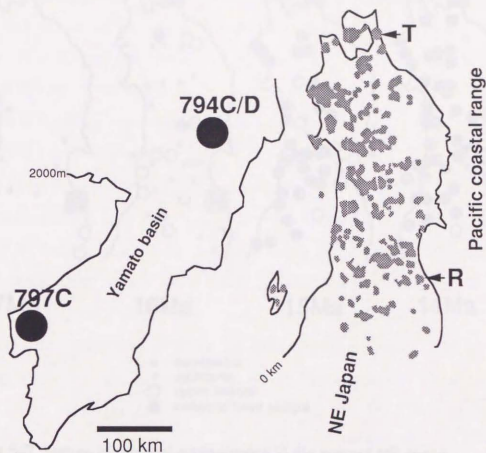


Fig.5-1. Distribution of the early to middle Miocene (23 to 14 Ma) volcanic central facies on the present NE Japan (Stippled areas; after Ohguchi et al., 1989). R and T denote Ryozen and Tomari districts, respectively. 797C and 794C/D denote locations of the cored basement in the Yamato basin (see §2-1).

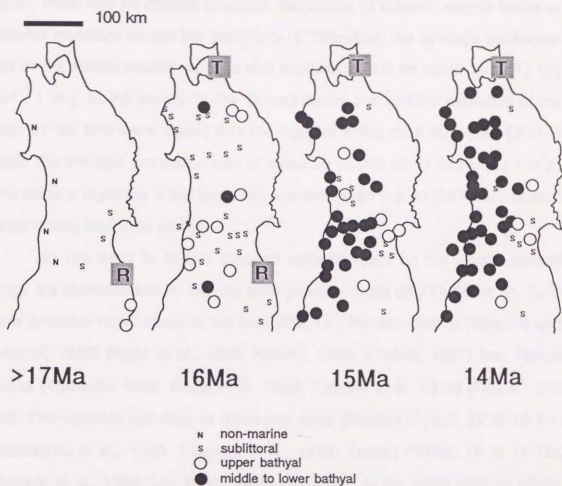


Fig.5-2. Nature of regional submergence in the present NE Japan during early to middle Miocene (after Yamaji, 1990). R and T denote Ryozen and Tomari districts, respectively.

1963; Ui, 1979). It yields the average production rate of about $10 \text{ km}^3 / 100 \text{ km}^2 / 1 \text{ m.y.}$ during the period. It should be noted that, on the early Neogene NE Japan, there was no change in spatial distribution of volcanic central facies or volcanic materials across the arc (Fig.5-1). Therefore, the average production rate on the Pacific coastal range is also approximated to be about $10 \text{ km}^3 / 100 \text{ km}^2 / 1 \text{ m.y.}$ in the period. In the Yamato basin, the igneous materials of the order of 10^5 km^3 were issued with the regional rifting for 5 m.y. (see §2-2). It yields the average production rate of about $20 \text{ to } 200 \text{ km}^3 / 100 \text{ km}^2 / 1 \text{ m.y.}$. This value is higher by a few factors to one-order than that on the Pacific coastal range during the same period.

(3) The early to middle Miocene volcanic rocks on the Pacific coastal range are characterized by bearing quite primitive rocks ($\text{MgO} \geq 10 \text{ wt.}\%$). Such quite primitive rocks occur at the two sites, i.e., Ryozen district (Ishizaka and Tatsumi, 1980; Shuto et al., 1985; Kotoku, 1986; Kushiro, 1987) and Tomari district (Takimoto, 1986; Shuto et al., 1988; Tatsumi et al., 1988) (Figs.5-1 and 5-2). The volcanic activities at those two sites (Ryozen district; 22 to 16 Ma; Tsunakawa et al., 1983; Ohguchi et al., 1989; Tomari district; 16 to 14 Ma; Ohguchi et al., 1989; Uto et al., 1989) took place at the same time as rifting-related volcanism in the Yamato basin estimated at 20 to 15 Ma (see §2-2).

In this chapter, the rifting-related basalt magma of the Yamato basin is compared with published petrological characteristics of the temporally-associated, but spatially-distinct primitive rocks from above two sites, and then distinct aspects in genesis of the primary magmas are discussed.

§5-2 Compositionally distinct primary magmas

Figure 5-3 shows normative whole rock compositions of the early to middle Miocene primitive rocks ($\text{MgO} \geq 10$ wt.%) from the Pacific coastal range together with the least differentiated rifting-related basaltic rocks ($\text{MgO} = 10$ wt.%) from the Yamato basin. The early to middle Miocene primitive rocks from the Pacific coastal range have olivine-tholeiite compositions defining well concentrated cluster in normative composition space. On the other hand, the least differentiated rifting-related basaltic rocks from the Yamato basin are definitely depleted in normative Qz component compared to them.

For the early to middle Miocene primitive olivine-tholeiites from the Pacific coastal range, major-element compositions of their parental primary magmas were estimated with back-track calculation of olivine maximum fractionation; the same method as that applied for the rifting-related basaltic rocks from the Yamato basin (see §3-4). Assumptions involved in the estimation are the followings:

(1) Liquid compositions of the early to middle Miocene primitive olivine-tholeiite magmas of the Pacific coastal range can be approximated by the published whole rock compositions of the primitive natural rocks. It is justified because the primitive rocks are predominantly olivine-phyric and the olivine phenocrysts are almost not accumulative (Shuto et al., 1985; Kotoku, 1986; Takimoto, 1986). The evidently olivine-accumulative rocks described by Kotoku (1986) were ignored in the estimation.

(2) Back-track calculation of olivine maximum fractionation can be applied. It may be valid because olivine is the dominant liquidus phase in the primitive rocks (Shuto et al., 1985; Kotoku, 1986; Takimoto, 1986).

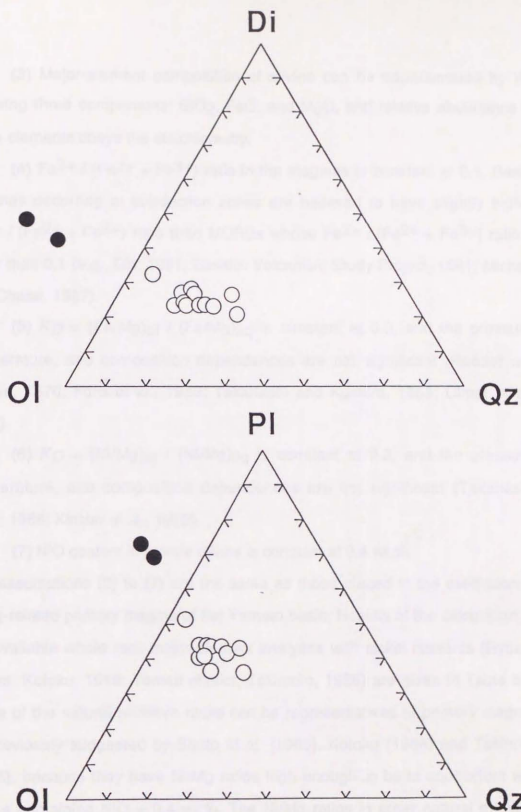


Fig.5-3. Normative projections of whole rock compositions of the early to middle Miocene primitive rocks ($MgO \geq 10$ wt.%) from the Pacific coastal range of the present NE Japan (○) and the least differentiated rifting-related basaltic rocks ($MgO = 10$ wt.%) from the Yamato basin (●). The projection method of Walker et al. (1979) was applied.

(3) Major-element composition of olivine can be approximated by the following three components: SiO_2 , FeO , and MgO , and relative abundance of these elements obeys the stoichiometry.

(4) $\text{Fe}^{3+} / (\text{Fe}^{2+} + \text{Fe}^{3+})$ ratio in the magmas is constant at 0.1. Basalt magmas occurring at subduction zones are believed to have slightly higher $\text{Fe}^{3+} / (\text{Fe}^{2+} + \text{Fe}^{3+})$ ratio than MORBs whose $\text{Fe}^{3+} / (\text{Fe}^{2+} + \text{Fe}^{3+})$ ratio is lower than 0.1 (e.g., Gill, 1981; Basaltic Volcanism Study Project, 1981; Michael and Chase, 1987).

(5) $K_D = (\text{Fe}/\text{Mg})_{\text{ol}} / (\text{Fe}/\text{Mg})_{\text{liq}}$ is constant at 0.3, and the pressure, temperature, and composition dependences are not significant (Roeder and Emslie, 1970; Ford et al., 1983; Takahashi and Kushiro, 1983; Ulmer et al., 1989).

(6) $K_D = (\text{Ni}/\text{Mg})_{\text{ol}} / (\text{Ni}/\text{Mg})_{\text{liq}}$ is constant at 2.3, and the pressure, temperature, and composition dependences are not significant (Takahashi, 1978; 1986; Kinzler et al., 1990).

(7) NiO content in mantle olivine is constant at 0.4 wt.%.

The assumptions (2) to (7) are the same as those placed in the estimation of rifting-related primary magma of the Yamato basin. Results of the calculation on the available whole rock major-element analyses with nickel contents (Ryozen district; Kotoku, 1986; Tomari district; Takimoto, 1986) are given in Table 5-1. Some of the natural primitive rocks can be representatives of primary magma, as previously suggested by Shuto et al. (1985), Kotoku (1986) and Takimoto (1986), because they have Ni/Mg ratios high enough to be in equilibrium with olivine containing NiO = 0.4 wt.%. The Ni/Mg ratios in other natural primitive ones are also very close to the value acceptable as that of primary magma; only little amounts of olivine (almost below 5 wt.%) are required to add them to raise the Ni/Mg ratios until the value high enough to be in equilibrium with olivine

	1	2	3	4	5	6	7	8	9	10	11	12	13
Sample ID	62101	83104	72910	71509	112610	72917	72911	61208	T92	T93	Average	IK85060803	797C12R4/35-37
SiO ₂	49.12	48.22	49.88	50.19	49.45	49.37	49.38	49.72	51.37	51.82	49.85	49.03	47.87
TiO ₂	0.88	0.83	0.81	0.84	0.52	0.58	0.51	0.50	0.51	0.52	0.57	0.84	0.87
Al ₂ O ₃	14.08	14.71	15.02	15.14	14.93	14.78	13.54	13.03	13.23	14.37	14.28	13.95	16.38
FeO*	9.46	8.74	9.15	9.70	9.28	9.22	9.57	9.19	9.44	8.40	9.22	8.95	7.57
MnO	0.17	0.18	0.18	0.18	0.17	0.16	0.17	0.17	0.14	0.14	0.16	0.15	0.15
MgO	14.24	15.45	12.34	11.20	13.17	13.27	14.41	14.91	13.38	11.46	13.38	12.38	10.98
CaO	10.18	10.25	10.41	10.75	10.41	10.37	10.74	10.19	9.73	10.57	10.38	10.75	10.23
Na ₂ O	1.79	1.82	2.15	1.88	1.78	1.95	1.53	1.93	1.72	1.98	1.83	1.93	2.81
K ₂ O	0.24	0.22	0.22	0.25	0.24	0.25	0.13	0.31	0.44	0.70	0.30	0.27	0.05
P ₂ O ₅	0.05	0.00	0.07	0.07	0.08	0.07	0.04	0.07	0.08	0.07	0.08	0.07	0.11
NiO(ppm)	510	520	440	420	460	480	510	520	480	410			500
FeO*/MgO	0.68	0.57	0.74	0.87	0.71	0.70	0.66	0.62	0.71	0.73	0.69	0.72	0.54
Fo% equilibrium Ol	91	92	90	88	90	91	91	92	90	90		89	92
NiO wt% equilibrium Ol	0.41	0.40	0.40	0.41	0.40	0.41	0.41	0.40	0.41	0.40			0.41
Added Ol wt.%	3	7	0	0	5	2	1	3	4	2		0	10

Table 5-1. Estimated early to middle Miocene primary basalt magmas of the Pacific coastal range of the present NE Japan and the primary rifting-related basalt magma of the Yamato basin. All the major-element compositions are recalculated to be total = 100 wt.%.

Columns 1 - 8: Estimations on the published whole rock XRF analyses on the primitive basalts (MgO > 10 wt.%) from the Ryozen district, NE Japan (Kotoku, 1986).

Columns 9 and 10: Estimation on the published whole rock XRF analyses on the primitive basalts (MgO > 10 Wt.%) from the Tomari district, NE Japan (Takimoto, 1986).

Column 11: Average of columns 1 - 10.

Column 12: Primitive basalt from the Ryozen district, NE Japan used as starting material in the high-pressure melting experiment of Kushiro (1987).

Column 13: Estimated primary rifting-related basalt magma of the Yamato basin (§3-4).

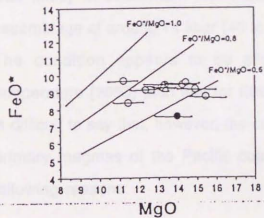
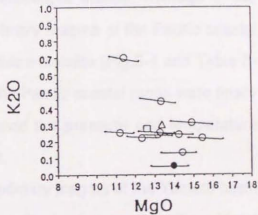
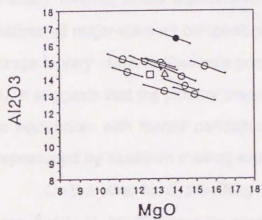
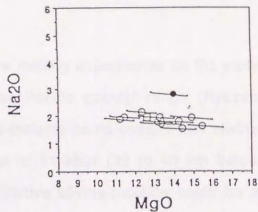
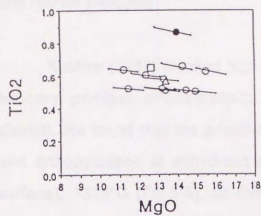
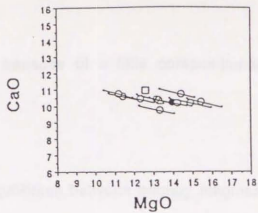
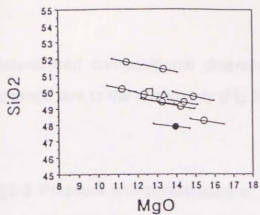
containing NiO = 0.4 wt.% (Table 5-1). The estimated major-element compositions of parental primary magmas of the Pacific coastal range are graphically shown in Fig.5-4. They show no significant compositional variations other than MgO varying from 11 to 15 wt.%.

The rifting-related primary magma of the Yamato basin appears to have had distinguishable major-element composition from the primary magmas of the Pacific coastal range (Fig.5-4 and Table 5-1), i.e., higher TiO₂, Al₂O₃, and Na₂O and lower SiO₂ and K₂O contents in the former than the latter. The discrepancies in their SiO₂, Al₂O₃ and Na₂O contents are principally a reflection of the distinct amounts of normative Qz component among the differentiated natural rocks (Fig.5-3). Also, FeO*/MgO ratio was lower in the former than in most of the latter.

Taking into account coherent behavior between K₂O and H₂O in basalt magma (e.g., Aoki et al., 1981), the higher amounts of K₂O in the latter might be a suggestive of somewhat higher amounts of magmatic H₂O in the latter. However, the K₂O contents are entirely very low (almost below 0.5 wt.%; Fig.5-4 and Table 5-1), suggesting that they were almost anhydrous with little magmatic H₂O < 1 wt.% according to Aoki et al. (1981).

Above interpretations are made assuming that the mantle olivines, which were finally in equilibrium with the magmas, contained constant NiO = 0.4 wt.% in both areas. Strictly speaking, real NiO content of mantle olivine scatters around 0.4 wt.% (± 0.05 wt.%; Sato, 1977; Elthon, 1989). It would change the amounts of olivine added to estimate the primary magmas, as described before (see §3-4). However, this kind of uncertainty does not much affect the

Fig.5-4. Major-element compositions of the estimated early to middle Miocene primary magmas of the Pacific coastal range of the present NE Japan (○). The estimated rifting-related primary magma of the Yamato basin (●) is also shown. All the estimations were made assuming NiO content of mantle olivine = 0.4 wt.%. Bars beside each symbols represent uncertainty in the estimations where NiO content of mantle olivine changes by 0.4 ± 0.05 wt.%. Averaged composition of the estimated primary magmas of the Pacific coastal range is shown by (△). The primitive olivine-tholeiite used in melting experiment of Kushiro (1987) is shown by (□). All the major-element compositions are recalculated to be total = 100 wt.%.



interpreted compositional discrepancies because of a little compositional change due to the uncertainty (Fig.5-4).

§5-3 Pressure and temperature of final equilibrium between primary magmas and mantle peridotite

Kushiro (1987) directed high-pressure melting experiments on the early Miocene primitive olivine-tholeiite from the Pacific coastal range (Ryozen district). He found that the primitive olivine-tholeiite could coexist with olivine and orthopyroxene at anhydrous condition of 11 kbar (30 to 40 km below surface), 1315°C (Fig.5-5), so that the primitive olivine-tholeiite could be a primary magma finally equilibrated with harzburgite mantle. Average of the estimated major-element compositions of primary magma of the Pacific coastal range is very close to Kushiro's primitive olivine-tholeiite (Fig.5-4 and Table 5-1). It suggests that the primary magmas of the Pacific coastal range were finally in equilibrium with mantle peridotite at *around* the pressure and temperature reproduced by Kushiro's melting experiment.

On the other hand, the rifting-related primary magma of the Yamato basin was finally in equilibrium with mantle peridotite having harzburgitic mineral assemblage at around 14 kbar (40 to 50 km below surface), 1340°C (see §4-4). The condition appears to be slightly higher in pressure (3 kbar) and temperature (20°C) than that for Kushiro's primitive olivine-tholeiite (Fig.5-5). It is difficult to say that, however, the condition was distinct from that for the entire primary magmas of the Pacific coastal range. This is principally due to the following reasons:

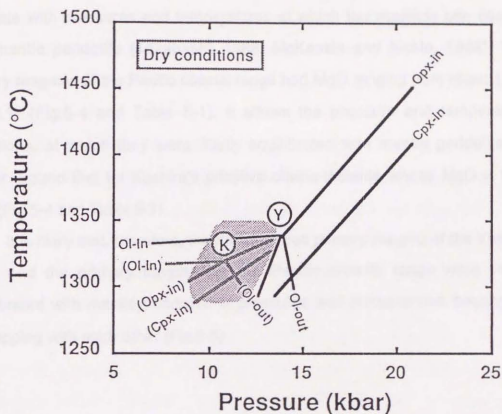


Fig.5-5. Experimentally obtained dry melting phase relations of the estimated rifting-related primary magma of the Yamato basin (Y: this study) and the early Miocene primitive olivine-tholeiite from the Pacific coastal range (K: Kushiro, 1987). Letters in parentheses denote phase relation for the latter. Stippled region denotes probable range of pressures and temperatures at which the primary magmas of the Pacific coastal range were finally in equilibrium with mantle peridotite (see text).

(1) The experimentally obtained pressures and temperatures of final equilibrium with mantle peridotite are proximate between the rifting-related primary magma of the Yamato basin and Kushiro's primitive olivine-tholeiite.

(2) In general, concentrations of MgO in primary magmas positively correlate with pressures and temperatures at which the magmas can coexist with mantle peridotite (Takahashi, 1986; McKenzie and Bickle, 1988). The primary magmas of the Pacific coastal range had MgO ranging from about 11 to 15 wt.% (Fig.5-4 and Table 5-1). It allows the pressure and temperature conditions, at which they were finally equilibrated with mantle peridotite, to scatter around that for Kushiro's primitive olivine-tholeiite whose MgO = 12.4 wt.% (Fig.5-4 and Table 5-1).

It is likely that, therefore, the rifting-related primary magma of the Yamato basin and the primary magmas of the Pacific coastal range were finally equilibrated with mantle peridotite at pressures and temperatures bearing an overlapping with each other (Fig.5-5).

§5-4 Origin of compositional discrepancies of primary magmas

The previous experimental works (Jaques and Green, 1980; Fujii and Scarfe, 1985) revealed that, in a single peridotite or peridotite/basalt system, melts coexisting with peridotitic mineral assemblages have lower TiO_2 , Al_2O_3 , and Na_2O contents and lower FeO^*/MgO ratio with increasing extent of partial melting. The rifting-related primary magma of the Yamato basin had definitely higher amounts of TiO_2 , Al_2O_3 , and Na_2O than the primary magmas of the Pacific coastal range (Fig.5-4 and Table 5-1). It might be a suggestive of lower extent of partial melting for the former than for the latter if compositionally

uniform source mantle peridotite was supposed for them. On the other hand, the rifting-related primary magma of the Yamato basin had lower FeO^*/MgO ratio than most of the primary magmas of the Pacific coastal range (Fig.5-4 and Table 5-1). It might suggest rather higher extent of partial melting for the former than for most of the latter if they were derived from compositionally uniform mantle peridotite. These internally-discordant suggestions mean that the compositional discrepancies of primary magmas between the areas could not be created by different extents of partial melting of compositionally uniform mantle peridotite. It is also suggested by the nearly overlapping equilibrium pressures and temperatures with mantle peridotites (Fig.5-5), which is unlikely to yield different extents of partial melting to compositionally uniform mantle peridotite.

Alternatively, the compositional discrepancies could result from partial melting of compositionally distinct mantle peridotites at nearly overlapping pressures and temperatures. This idea is justified because of the followings: Partial melting of natural (therefore, multi-component) mantle peridotite can not be isobarically invariant, so that composition of primary magma depends on composition of the source mantle peridotite other than pressure and temperature (Jaques and Green, 1980; Bryan and Dick, 1982; Fujii and Bougault, 1983; Dick et al., 1984; Fujii and Scarfe, 1985; Presnall and Hoover, 1987). We do not have any direct informations of compositions of the mantle peridotites beneath the areas of interest, particularly beneath the Yamato basin as mentioned in the previous section (§3-4). It means that compositional uniformity in the source mantle peridotites between the areas can not be proved at the moment. On the contrary, mantle-derived peridotite xenoliths bear significant compositional variations depending on geological settings and locality (e.g., Boyd and McCallister, 1976; Maaloe and Aoki, 1977; Jordan, 1979; Anderson, 1989; Boyd, 1989).

In order to examine nature of the compositional discrepancy of source mantle peridotites between the areas, the possible compositional ranges were estimated for both of the rifting-related primary magma of the Yamato basin and the *average* primary magma of the Pacific coastal range in terms of FeO^*/MgO ratio.

The *average* primary magma of the Pacific coastal range can be in equilibrium with harzburgite mantle because of the following reasons: (1) The *average* primary magma has major-element composition very close to Kushiro's primitive olivine-tholeiite (Fig.5-4 and Table 5-1). (2) Kushiro's primitive olivine-tholeiite was experimentally proved to can coexist with harzburgite mantle (Kushiro, 1987) (Fig.5-5). It is considered that, on the other hand, the rifting-related primary magma of the Yamato basin was finally in equilibrium with harzburgite mantle (Fig.5-5). Therefore, bulk compositions of the respective source mantle peridotites should be expressed by mixing of the following three components; the magma, olivine, and orthopyroxene, among which chemical equilibrium are achieved with each other. Compositions of the coexisting olivines and orthopyroxenes were calculated based on the following assumptions;

(1) Chemical compositions of olivine and orthopyroxene can be approximated by the three components; SiO_2 , FeO , and MgO , and their relative abundance obeys respective stoichiometry.

(2) $K_D = (\text{Fe}/\text{Mg})_{\text{ol}} / (\text{Fe}/\text{Mg})_{\text{liq}}$ is constant at 0.3 (e.g., Roeder and Emslie, 1970; Ford et al., 1983; Takahashi and Kushiro, 1983; Ulmer, 1989).

(3) $K_D = (\text{Fe}/\text{Mg})_{\text{ol}} / (\text{Fe}/\text{Mg})_{\text{opx}}$ is constant at 1.0 (e.g., Matsui and Nishizawa, 1974; Brown, 1982).

(4) $\text{Fe}^{3+} / (\text{Fe}^{2+} + \text{Fe}^{3+})$ in the magmas is constant at 0.1.

Figure 5-6 shows calculated compositions of the olivines and orthopyroxenes in FeO^* variations against MgO together with coexisting magmas. Possible compositional range of the source mantle peridotite for the rifting-related primary magma of the Yamato basin is well displaced toward Fe-poor compositions from that for the *average* primary magma of the Pacific coastal range.

If the rifting-related primary magma of the Yamato basin was produced by 30 % melting (in weight fraction), the hypothetical source mantle peridotite might have similar bulk FeO^*/MgO ratio to the calculated *residual* harzburgite mantle for the *average* primary magma of the Pacific coastal range (Fig.5-6). In other words, difference in melting extents (ΔX) between them should be above 30 % (in weight fraction), supposing higher bulk FeO^*/MgO for the former's source mantle peridotite. It is not likely because of the following reason: According to the variation of residual mineral assemblages as a function of the melting extents; experimentally obtained in a wide range of compositions of peridotites (Mysen and Kushiro, 1977; Jaques and Green, 1980), this kind of largely different ΔX ($\geq 30\%$) yields different residual mineral assemblages. In reality, however, identical residual mineral assemblage (harzburgitic) is likely for both primary magmas as mentioned above.

The above considerations may suggest that the mantle peridotite with lower bulk FeO^*/MgO ratio (therefore, more refractory) was dominant as source for the rifting-related primary magma of the Yamato basin as compared to for the primary magmas of the Pacific coastal range. In general sense, refractory mantle peridotite with lower bulk FeO^*/MgO ratio yields lower extent of partial melting at a given pressure and temperature condition (e.g., Mysen and Kushiro, 1977). As mentioned, the rifting-related primary magma of the Yamato

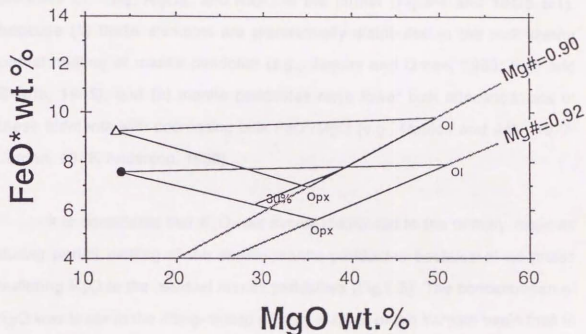


Fig.5-6. FeO-MgO constraint on bulk compositions of the source mantle peridotites for the rifting-related primary magma of the Yamato basin (●) and the average primary magma of the Pacific coastal range (Δ). The triangles are comprised by the coexisting primary magma, olivine, and orthopyroxene which are in equilibrium with each other. Bulk compositions of each source mantle peridotites should have been lie within the respective triangles because the primary magmas were finally in equilibrium with harzburgite residual mantles (see text). If the rifting related primary magma of the Yamato basin was produced by 30% melting, bulk composition of the hypothetical source mantle peridotite should be on the line labeled by 30%. The further implication is given in text.

basin and the primary magmas of the Pacific coastal range were finally equilibrated with mantle peridotite at nearly overlapping pressures and temperatures (Fig.5-5). Accordingly, the rifting-related primary magma of the Yamato basin was produced by lower extent of partial melting than the primary magmas of the Pacific coastal range. This is not inconsistent with the higher amounts of TiO_2 , Al_2O_3 , and Na_2O in the former (Fig.5-4 and Table 5-1), because (1) these elements are preferentially distributed to the melt during partial melting of mantle peridotite (e.g., Jaques and Green, 1980; Fujii and Scarfe, 1985), and (2) mantle peridotites have lower bulk concentrations of these elements with decreasing bulk FeO^*/MgO (e.g., Maaloe and Aoki, 1977; Jordan, 1979; Anderson, 1989).

It is considered that K_2O was almost distributed to the primary magmas during partial melting of the source mantle peridotites because of no phase buffering K_2O in the residual mantle peridotites (Fig.5-5). The concentration of K_2O was lower in the rifting-related primary magma of the Yamato basin than in the primary magmas of the Pacific coastal range (in the former, one-fourth or less as much as in the latter; Fig.5-4 and Table 5-1). It may be inconsistent with the lower extent of partial melting for the former suggested above. Otherwise, it may be a suggestive of preferential K_2O -enrichment in the source mantle peridotite for the latter.

K^+ exhibits a distinct behavior from other major-element cations under presence of H_2O fluid, because K^+ has both large ionic radius and low valence, unlike other major-element cations, which make it soluble to H_2O fluid. Therefore, the source mantle peridotite beneath the Pacific coastal range might be preferentially enriched in K_2O if it was flushed by H_2O fluid carrying K^+ . It is generally understood that, in subduction zones, dehydration of subducting

oceanic slab supplies K⁺-bearing H₂O fluid to the overlying wedge mantle (e.g., Sakuyama and Nesbitt, 1986; Tatsumi, 1986; Tatsumi et al., 1986). The continental margin of the eastern Asia was continuously placed under the situation with westward subduction of Pacific plate throughout Neogene (e.g., Rea and Duncan, 1986; Maruyama et al., 1989). Therefore, it is likely that the source mantle peridotite beneath the early to middle Miocene Pacific coastal range was flushed by the slab-derived K⁺-bearing H₂O fluid. On the contrary, the source mantle peridotite for the rifting-related primary magma of the Yamato basin was probably not much flushed by such H₂O fluid.

Accordingly, the compositional discrepancies between the rifting-related primary magma of the Yamato basin and the primary magmas of the Pacific coastal range probably resulted from the following; (1) compositionally distinct source mantle peridotites, and (2) the resulted distinct extent of partial melting at nearly overlapping pressures and temperatures. Contents of the distinctness are summarized in Table 5-2 together with other significant differences between the magmatic activities.

	Yamato basin	Pacific coastal range
<u>Source mantle peridotite</u>		
bulk FeO*/MgO ratio	lower (more refractory)	higher (less refractory)
slab-derived H ₂ O fluid	none	flushed
<u>Primary magma</u>		
final equilibrium pressure with residual mantle	around 14 kbar	around 11 kbar*
final equilibrium temperature with residual mantle	around 1340°C	around 1315°C*
extent of partial melting	lower	higher
composition	high-Al basalt	olivine-tholeiite
<u>Significance in volcanic activity</u>		
geological setting	rifted active continental margin	active continental margin
issued igneous materials	ca.20-200km ³ /100km ² /m.y.	ca.10km ³ /100km ² /m.y.

Table 5-2. Origin of compositional discrepancies between the rifting-related primary magma of the Yamato basin and the primary magma of the Pacific coastal range during early to middle Miocene.

*: The condition is likely for the "average" primary magma of the Pacific coastal range. Actual conditions are probably extended to both of the higher-pressures and temperatures and the lower-pressures and temperatures.

Chapter 6 Discussion: Implication for deep-seated physicochemical structure beneath rift

As mentioned first, the Yamato basin was created by regional rifting at active margin of the eastern Asian continent. In this chapter, a possible deep-seated physicochemical structure beneath the rift is proposed taking into account the petrological significance of the rifting-related basalt magma discussed in the previous chapters. The petrological significance of the rifting-related basalt magma is summarized as the followings:

(1) In terms of major-element chemistry, petrographical and compositional variations of the entire rifting-related basalt magmas were derived by crystallization differentiation of the identical parental magma at relatively low pressures.

(2) The parental primary magma had high-Al basalt composition with MgO around 14 wt.%. It was finally in equilibrium with harzburgite mantle at anhydrous condition around 14 kbar (40 to 50 km below surface), 1340°C.

(3) The parental primary magma had distinct major-element composition from the temporally-associated primary magma of the Pacific coastal range where considerable stretching of the lithosphere did not occur in the period. This difference principally resulted from refractory nature of the source mantle peridotite and the resulted lower extent of partial melting for the rifting-related primary magma.

Abe and Kanamori (1970) and Evans et al. (1978) proposed shallow top of low velocity channel (30 to 50 km below surface) beneath the *present* basinal area (Abe and Kanamori, 1970; Evans et al., 1978) (Fig.6-1). It may suggest

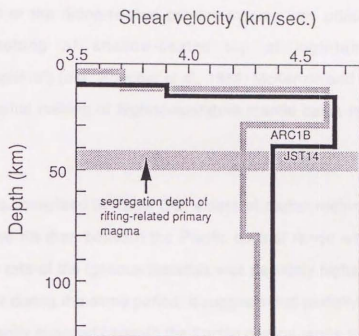


Fig.6-1. Shear velocity structure models beneath the *present* basinal area of the Japan Sea. Two representative ones (JST14 and ARC1B) are shown after Evans et al. (1978). Note that the shallow-seated top of low-velocity channel nearly corresponds to the segregation depth of the rifting-related primary magma.

that, during early to middle Miocene, the upper most mantle itself beneath the area was at temperature high enough to melt it partially. As discussed in Chapter 4, the experimental evidence suggests that the depth, at which the rifting-related primary magma was released from the residual mantle, is around 40 to 50 km below surface. This depth is quite consistent with the shallow-seated top of the low velocity channel (Fig.6-1). Accordingly, it is likely that the generation of the rifting-related primary magma was principally governed by partial melting of shallow-seated top of high-temperature mantle ("asthenosphere") (e.g., Foucher et al., 1982; McKenzie and Bickle, 1988) rather than by partial melting of high-temperature mantle batch uprising sporadically ("diapir").

As summarized in Table 5-2, extent of partial melting was rather lower beneath the rift than beneath the Pacific coastal range whereas the average production rate of the igneous materials was definitely higher in the former than in the latter during the same period. It suggests that partially molten mantle was less frequently supplied beneath the Pacific coastal range than beneath the rift. Therefore, generation of the primary magma of the Pacific coastal range is likely to have been governed by partial melting of high-temperature mantle batch uprising sporadically ("diapir"). The batch probably uprose from deeper-portion in the mantle wedge because of the following: Beneath the Pacific coastal range, the source mantle peridotite of primary magma was effectively flushed by slab-derived H₂O fluid (Table 5-2). Such polluted peridotite is believed to have been initially developed at deeper-portion in the mantle wedge immediately above the down-going slab (e.g., Tatsumi, 1986).

It is emphasized here that, as discussed in Chapter 5, the source mantle peridotite of primary magma was dominated by less refractory peridotite

beneath the Pacific coastal range as compared to beneath the rift (Table 5-2). Therefore, at least the deeper-portion of the mantle wedge is required to have been comprised of such less refractory peridotite. It leads the following two possibilities with respect to origin of the refractory peridotite created the rifting-related primary magma:

(1) The refractory peridotite was injected as high-temperature mass ("asthenosphere") from somewhere deep into the mantle wedge which was originally comprised of the less refractory peridotite. The injection was spatially-associated with the regional rifting.

(2) The refractory peridotite originally comprised upper portion of the high-temperature mantle ("asthenosphere") in the mantle wedge. The refractory peridotite was underlain by the less refractory high-temperature mantle peridotite from which the high-temperature batch ("diapir") uprose beneath the Pacific coastal range.

At present, the latter possibility is more likely because of the following reasons: (1) It is generally understood that, beneath continents, refractory peridotite is underlain by less refractory peridotite (e.g., Boyd and McCallister, 1976; Oxburgh and Parmentier, 1978; Jordan, 1979; Anderson, 1989; Boyd, 1989). (2) Generation of the rifting-related primary magma was probably governed by partial melting of the shallow-seated top of high-temperature mantle ("asthenosphere") itself, as discussed above. Therefore, it is not necessary that the high-temperature mantle beneath the rift uprose from deeper-portion in the mantle wedge, unlike beneath the Pacific coastal range.

Based on the above discussions, a possible petrological model for the deep-seated physicochemical structure beneath the rift can be drawn as Figs. 6-2(A) and (B). According to the present model, the upper mantle beneath the rift

was compositionally layered, i.e., refractory peridotite was underlain by less refractory peridotite (Fig.6-2(A)). It is considered that the compositional boundary was deeper-placed than the boundary between the stretched or detached low-temperature rigid mantle ("lithosphere") and the high-temperature mantle ("asthenosphere").

Uppermost portion of the refractory high-temperature mantle partially melted (Fig.6-2(A)) due to the emplacement at lower in pressures and higher in temperatures than the appropriate solidus, likely associated with the regional stretching and probable detachment of the overlying low-temperature rigid mantle. As discussed in Chapter 4, the rifting-related primary magma probably segregated from the residual mantle at around 1340°C, 40 km to 50 km below surface (Fig.6-2(B)). Temperature of partially molten mantle drastically increases with increasing pressure (depth) due to the effect of the latent heat of melting (e.g., Verhoogen, 1973; McKenzie, 1984; Fukuyama, 1985; McKenzie and Bickle, 1988). Therefore, the refractory high-temperature mantle probably had temperatures above ca. 1300°C everywhere. This kind of shallow-seated high-temperature mantle beneath the rift was previously predicted by several workers (e.g., Nohda et al., 1988; Tatsumi et al., 1989) based on the petrologically estimated thermal structure beneath the early to middle Miocene NE Japan and the extrapolation to beneath the basinal area of the Japan Sea.

Assuming the convective (isentropic) thermal gradient and the "average" mantle solidus (McKenzie, 1984; McKenzie and Bickle, 1988) for the high-temperature mantle, the partial melting might be attained downward until the depth around 80 km where temperature was around 1450°C (Fig.6-2(B)). It should be noted here that convective geotherm is not assured in the system whose thickness is restricted (e.g., Verhoogen, 1973). This is likely in the refractory high-temperature mantle which was probably underlain by the less

refractory high-temperature mantle within the mantle wedge. In this case, the possible conductive heat loss might yield the condition, at which downward limit of the partial melting was defined, rather higher in both pressure (depth) and temperature.

The underlying less refractory high-temperature mantle is unlikely to have melted, because the entire rifting-related basaltic rocks from the Yamato basin were probably derived from the identical parental primary magma, i.e., partial melt of the refractory high-temperature mantle. It may suggest that the refractory high-temperature mantle was underlain by the less refractory high-temperature mantle at some depth well below ca. 80 km (Fig.6-2(A)).

References

- Abe, K. and Kanamori, H. (1970) Mantle structure beneath the Japan Sea as revealed by surface waves. *Bull. Earthq. Res. Inst. Univ. Tokyo*, 48, 1011-1021.
- Anderson, D.L. (1989) *Theory of the Earth*. U.K., Backwell Scientific Pub., 179-196p.
- Ando, A., Mita, N., and Terashima, S. (1987) 1986 values for fifteen GSJ rock reference samples, "igneous rock series". *Geostandard Newslett.*, 11, 159-166.
- Aoki, K., Ishiwaka, K., and Kanisawa, S. (1981) Fluorine geochemistry of basaltic rocks from continental and oceanic regions and petrogenetic application. *Contrib. Mineral Petrol.*, 76, 53-59.
- Aramaki, S. (1987) Geological background of the lethal gas burst from Lake Nyos, Cameroon, August 1986. *Bull. Volcanol. Soc. Japan*, 32, 57-72 (Japanese with English abstract).
- Baker, D.R. and Eggler, D.H. (1983) Fractionation paths of Atka (Aleutian) high-alumina basalt: Constraints from phase relations. *J. Volcanol. Geotherm. Res.*, 18, 387-404.
- Baker, D.R. and Eggler, D.H. (1987) Compositions of anhydrous and hydrous melts coexisting with plagioclase, augite, and olivine or low-Ca pyroxene from 1 atm to 8 kbar: Application to the Aleutian volcanic center of Atka. *Amer. Mineral.*, 72, 12-28.
- Basaltic Volcanism Study Project (1981) *Basaltic volcanism on the terrestrial planets*. Pergamon Press, Inc., New York.
- Bence, A.E. and Albee, A.L. (1968) Empirical correction factors for the electron microanalysis of silicates and oxides. *J. Geol.*, 76, 382-403.

- Bottinga, Y. and Weill, D.F. (1970) Densities of liquid silicate systems calculated from partial molar volumes of oxide components. *Amer. J. Sci.*, 269, 169-182.
- Boyd, F.R., Bell, P.M., England, J.L., and Gilbert, M.C. (1967) Pressure measurement in single-stage apparatus. *Carnegie year book*, 65, 410-414.
- Boyd, F.R. and McCallister, R.H. (1976) Densities of fertile and sterile garnet peridotite. *Geophys. Res. Lett.*, 3, 509-512.
- Boyd, F.R. (1989) Compositional distinction between oceanic and cratonic lithosphere. *Earth Planet. Sci. Lett.*, 96, 15-26.
- Brown, G.E. (1982) Olivines and silicate spinels. In: Ribbe, P.H. (editor), *Reviews in mineralogy*, 5, *Orthosilicates*, 342-344p.
- Bryan, W.B. and Moore, J.G. (1977) Compositional variations of young basalts in the Mid-Atlantic Ridge rift valley near lat. 36°49'N. *Bull. Geol. Sci. Amer.*, 88, 556-570.
- Bryan, W.B. and Dick, H.J.B. (1982) Contrasted abyssal basalt liquidus trends: evidence for mantle major element heterogeneity. *Earth. Planet. Sci. Lett.*, 58, 15-26.
- Burnham, C.W. and Davis, N.F. (1969) Partial molar volume of water in albite melts. *Amer. Geophys. Union Trans.*, 50, 338.
- Celaya, M. and McCabe, R. (1987) Kinematic opening of the Sea of Japan and the bending of the Japanese Island. *Geology*, 15, 53-57.
- Coleman, R.G. and McGuire, A.V. (1988) Magma systems related to the Red Sea opening. *Tectonophysics*, 150, 77-100.

- Dick, H.J.B., Marsh, N.G., and Bullen, T.D. (1980) Abyssal basalts from the Shikoku basin: their petrology and major element geochemistry. In: Klein, G. de V., Kobayashi, K., et al. *Init.Repts,DSDP*, 58, Washington (U.S. Govt.Printing Office), 843-872.
- Dick, H.J.B., Fisher, R.L., and Bryan, W.B. (1984) Mineralogic variability of the uppermost mantle along mid-ocean ridges. *Earth.Planet.Sci.Lett.*, 69, 88-106.
- Einsele, G. (1982) Mechanism of sill intrusion into soft sediment and exsolution of pore water. In: Curray, J.R. and Moore, D.G. et al., *Init.Repts.DSDP*, 64, Washington (U.S. Govt.Printing Office), 1169-1179.
- Elthon, D. (1983) Isomolar and isostructural pseudo-liquidus phase diagrams for oceanic basalts. *Amer.Mineral.*, 68, 506-511.
- Elthon, D. (1989) Pressure of origin of primary mid-oceanic ridge basalts. In: (editors.) Saunders, A.D. and Norry, M.J. *Magmatism in the ocean basins.*, Geol.Soc.Special Pub.42, Oxford, London, 125-136p.
- Evans, J.R., Suyehiro, K., and Sack, I.S. (1978) Mantle structure beneath the Japan Sea - a re-examination. *Geophys.Res.Lett.*, 5, 487-490.
- Fisher, R.V. and Schmincke, H.-U. (1984) *Pyroclastic rocks*. Springer-Verlag, Berlin, 267-270p.
- Ford, C.E., Russel, D.G., Graven, J.A., and Fisk, M.R. (1983) Olivine liquid equilibria; temperature, pressure, and composition dependence of the crystal/liquid cation partition coefficients for Mg, Fe²⁺, Ca, and Mn. *J.Petrol.*, 24, 256-265.
- Foucher, J.P., Le Pichon, X., and Sibuet, J.C. (1982) The ocean-continent transition in the uniform lithospheric stretching model: role of partial melting in the mantle. *Phil.Trans.R.Soc.Lond.*, A305, 27-43.

- Fujii, T., Kushiro, I., and Hamuro, K. (1978) Melting relation and viscosity of an abyssal olivine tholeiite. In: Meison, W.G. and Rabinowitz, P.D., *Init.Rept.Deep Sea Drilling Project XLV*, Washington., 513-517.
- Fujii, T. and Bougault, H. (1983) Melting relations of a magnesian abyssal tholeiite and the origin of MORBs. *Earth Planet.Sci.Lett.*, 62, 283-295.
- Fujii, T. and Scarfe, C.M. (1985) Composition of liquids coexisting with spinel lherzolite at 10 kbar and the genesis of MORBs. *Contrib.Mineral.Petrol.*, 90, 18-28.
- Fukuyama, H. (1985) Heat of fusion of basaltic magma. *Earth Planet.Sci.Lett.*, 73, 407-414.
- Gill, J.B. (1981) *Orogenic andesites and plate tectonics*. Springer-Verlag, Berlin.
- Green, D.H., Hibberson, W.O., and Jaques, A.L. (1979) Petrogenesis of mid-ocean ridge basalts. In: McElhinny, M.W. *The earth: Its origin, structure and evolution.*, 265-299p.
- Grove, T.L. (1981) Use of FePt alloys to eliminate the iron loss problem in 1 atmosphere gas mixing experiments: Theoretical and practical considerations. *Contrib.Mineral.Petrol.*, 78, 298-304.
- Grove, T.L., Kinzler, R.J., and Bryan, W.B. (1990) Natural and experimental phase relations of lavas from Seocki volcano. In: Detrick, R., Honnorez, J., Bryan, J., and Jeteau, T., et al., *Proc.ODP, Sci.Results*, 106/109. College Station, TX (Ocean Drilling Program), 9-18.
- Hawkins, J.W. and Melchior, J.T. (1985) Petrology of Mariana Trough and Lau Basin basalts. *J.Geophys.Res.*, 90, 11431-11468.
- Hilde, T.W. and Wageman, J.M. (1973) Structure and origin of the Japan Sea. In: Coleman, P.J. (ed.), *The western Pacific: Island arcs, marginal seas, geochemistry*. Univ.Western Australia Press, Perth, 415-434p.

- Huebner, J.S. (1971) Buffering techniques for hydrostatic systems at elevated pressures. In: *Research techniques for high pressure and high temperature*. Springer-Verlag, Berlin., 123-177.
- Hirata, N., Tokuyama, H., and Chung, T.W. (1989) An anomalously thick layering of the crust of the Yamato basin, southeastern Sea of Japan: the final stage of back-arc spreading. *Tectonophys.*, 165, 303-314.
- Honza, E., Inoue, M., Joshima, M., Knaya, H., Kato, M., Koizumi, I., Miyazaki, T., Murakami, F., Nishimura, K., Okamoto, K., Sugisaki, R., Tamaki, K., Terashima, T., and Yuasa, M. (1979) Geological investigation of the Japan Sea. In: *Cruise Rept. Geol. Surv. Japan*, 13.
- Ingle, J.C., Jr., Suyehiro, K., and von Breymann, M.T. et al. (1990) *Proc. ODP, Init. Repts.*, 128. College Station TX (Ocean Drilling Program).
- Isezaki, N. (1986) A magnetic anomaly map of the Japan Sea. *J. Geomag. Geoelectr.*, 38, 403-410.
- Ishizaka, K. and Tatsumi, Y. (1980) On trace element contents of some Ryozen volcanic rocks from the northeastern part of Fukushima Prefecture - A preliminary report -. *J. Japan. Assoc. Mineral. Petrol. Econ. Geol.*, 81, 312-323.
- Jaques, A.L. and Green, D.H. (1980) Anhydrous melting of peridotite at 0-15 kb pressure and the genesis of tholeiitic basalts. *Contrib. Mineral Petrol.*, 73, 287-310.
- Jordan, T.H. (1979) Mineralogy, density, and seismic velocity of garnet lherzolites and their geophysical implications. In: *The mantle sample: inclusions in kimberlites and other volcanics*. (editors) Boyd, F.R. and Meyer, H.O.A., Washington, D.C., Amer. Geophys. Union, 1-14p.

- Kaneoka, I., Notsu, K., Takigami, Y., Fujioka, K., and Sakai, H. (1990) Constraints on the time of the Japan Sea based on ^{40}Ar - ^{39}Ar ages and Sr isotopic ratios for volcanic rocks of Yamato Seamount Chain in the Japan Sea. *Earth Planet. Sci. Lett.*, 97, 211-225.
- Kaneoka, I., Takigami, Y., Takaoka, N., Yamashita, S., and Tamaki, K. ^{40}Ar - ^{39}Ar analyses of volcanic rocks drilled from the Japan Sea floor by Leg 127/128. (in preparation).
- Kinzler, R.J., Grove, T.L., and Recca, S.I. (1990) An experimental study on the effect of temperature and melt composition on the partitioning of nickel between olivine and silicate melt. *Geochim. Cosmochim. Acta*, 54, 1255-1265.
- Kobayashi, K. (1983) Spreading of the Sea of Japan and drift of Japanese Island Arc. *Mining Geol. Spec. Issue*, 11, 23-36 (in Japanese with English abstract).
- Kobayashi, K. (1988) *Preliminary report of the Hakuho-MarU cruise KH86-2*. Ocean Res. Inst. Univ. Tokyo., 67-74p.
- Konda, T. (1974) Bimodal volcanism in the Northeast Japan. *J. Geol. Soc. Japan*, 80, 81-89 (Japanese with English abstract).
- Kotoku, M. (1986) Geology and petrology of the Ryozen volcanic rocks. M. Thesis, Geological Inst., Univ. Tokyo.
- Kuno, H. (1960) High-alumina basalt. *J. Petrol.*, 1, 121-145.
- Kuno, H. (1966) Lateral variation of basalt magma type across continental margins and island arcs. *Bull. Volc.*, 29, 195-222.
- Kushiro, I. (1980) Viscosity, density, and structure of silicate melts at high pressures, and their petrological applications. In: Hargraves, R.B. *Physics of magmatic processes.*, 113p.

- Kushiro, I. (1987) A petrological model of the mantle wedge and lower crust in the Japanese island arcs. In: Mysen, B.O. (editor) *Magmatic processes: physicochemical principles*, 165-181p.
- Langmuir, C.H., Bender, J.F., Bence, A.E., and Hanson, G.N. (1977) Petrogenesis of basalts from the FAMOUS area: Mid-Atlantic Ridge. *Earth. Planet. Sci. Lett.*, 36, 133-156.
- Ludwig, L.A., Murauchi, S., and Houtz, R.E. (1975) Sediments and structure of the Japan Sea. *Geol. Soc. Amer. Bull.*, 86, 651-664.
- Maaloe, S. and Aoki, K. (1977) The major element composition of the upper mantle estimated from the composition of lherzolites. *Contrib. Mineral. Petrol.*, 63, 161-173.
- Maruyama, S., Liou, J.G., and Seno, T. (1989) Mesozoic and Cenozoic evolution of Asia. In: Zvi Bon-Avraham (editor), *The evolution of the Pacific ocean basins*. Oxford Univ. Press, 75-99p.
- Matsui, Y. and Nishizawa, O. (1974) Iron (II) - magnesium exchange equilibrium between olivine and calcium-free pyroxene over a temperature range 800°C to 1300°C. *Bull. Soc. Fr. Mineral. Crystallogr.*, 97, 122-130.
- McKenzie, D. (1984) The generation and compaction of partially molten rock. *J. Petrol.*, 25, 713-765.
- McKenzie, D. and Bickle, M.J. (1988) The volume and compaction of melt generated by extension of the lithosphere. *J. Petrol.*, 29, 625-679.
- Melson, W.G., Vallier, T.L., Wright, T.L., Byerly, G.R., and Nelen, J.A. (1977) A catalog of major element chemistry of abyssal volcanic glasses. *Smithson Contrib. Earth Sci.*, 19, 31-60.
- Michael, P.J. and Chase, R.L. (1987) The influence of primary magma composition, H₂O and pressure on Mid-Ocean Ridge basalt differentiation. *Contrib. Mineral. Petrol.*, 96, 245-263.

- Moore, D.G. and Curray, J.R. (1982) Geologic and tectonic history of the gulf of California. In: Curray, J.R. and Moore, D.G. et al., *Init. Repts. DSDP, 64*, Washington (U.S. Govt. Printing Office), 1279-1294.
- Mysen, B.O. and Kushiro, I. (1977) Compositional variations of coexisting phases with degree of melting of peridotite in the upper mantle. *Amer. Mineral.*, 62, 843-865.
- Nafziger, R.H., Ulmer, G.C., and Woermann, E. (1971) Gaseous buffering for the control of oxygen fugacity at one atmosphere. In: *Research techniques for high pressure and high temperature*. Springer-Verlag, Berlin., 9-41p.
- Niitsuma, N., Saito, Y., and Taira, A. (1988) Reconstruction of the Japanese islands before Japan Sea opening. *J. Phys. Earth*, 36, S133-S142.
- Nohda, S., Tatsumi, Y., Otofujii, Y., Matsuda, T., and Ishizaka, K. (1988) Asthenospheric injection and back arc opening: isotopic evidence from NE Japan. *Chemical. Geol.*, 68, 317-327.
- O'Donnel, T.H. and Presnall, D.C. (1980) Chemical variations of the glass and mineral phases in basalts dredged from 25-30°N along the mid-Atlantic ridge. *Amer. J. Sci.*, 280A, 845-868.
- Ohguchi, T., Yoshida, T., and Okami, K. (1989) Historical change of the Neogene and Quaternary volcanic field in the Northeast Honshu arc, Japan. *Memoir. Geol. Soc. Japan*, 32, 431-455 (Japanese with English abstract).
- Otofujii, Y., Hayashida, A., and Torii, M. (1985) When was the Japan Sea opened?: Paleomagnetic evidence from southwest Japan. In: N. Nasu et al. (editors), *Formation of active ocean margins*. Terra Pub., Tokyo, 551-556p.
- Oxburgh, E.R. and Parmentier, E.M. (1978) Thermal processes in the formation of continental lithosphere. *Phil. Trans. R. Soc. Lond.*, A288, 415-429.

- Presnall, D.C. and Hoover, J.D. (1984) Composition and depth of origin of primary mid-ocean ridge basalts. *Contrib. Mineral. Petrol.*, 87, 170-178.
- Presnall, D.C. and Hoover, J.D. (1987) High pressure phase equilibrium constraints on the origin of mid-ocean ridge basalts. In: Mysen, B.O. (editor) *Magmatic processes: physicochemical principles*, 75-89p.
- Rea, D.K. and Duncan, R.A. (1986) North Pacific plate convergence: a quantitative record of the past 140 m.y.. *Geology*, 14, 373-376.
- Roeder, P.L. and Emslie, R.F. (1970) Olivine-liquid equilibrium. *Contrib. Mineral. Petrol.*, 29, 275-289.
- Sakuyama, M. and Nesbitt, R.W. (1986) Geochemistry of the Quaternary volcanic rocks of the Northeast Japan arc. *J. Volcanol. Geotherm. Res.*, 29, 413-450.
- Sato, H. (1977) Nickel content of basaltic magmas: identification of primary magmas and a measure of the degree of olivine fractionation. *Lithos*, 10, 113-120.
- Saunders, A.D., Tarney, J., Stern, C.R., and Dalziel, I.W.D. (1979) Geochemistry of Mesozoic marginal basin floor igneous rocks from southern Chile. *Geol. Soc. Amer. Bull.*, 90, 237-258.
- Saunders, A.D. and Tarney, J. (1984) Geochemical characteristics of basaltic volcanism within back-arc basins. In: Kokelaar, B.P. and Howells, M.F. (editors.), *Marginal basin geology*. Oxford U.K., 59-76p.
- Shuto, K., Yashima, R., and Takimoto, T. (1985) Primitive olivine tholeiite from the Ryozen district, northeastern part of Fukushima Prefecture, Northeast Japan. *J. Japan. Assoc. Mineral. Petrol. Econ. Geol.*, 80, 55-72.

- Shuto,K., Takimoto,T., Sakai,A., Yamazaki,T., and Takahashi,T. (1988) Geochemical variation of with time of the Miocene volcanic rocks in northern part of the Northeast Japan arc. *Jour.Geol.Soc.Japan*, 94, 155-172 (Japanese with English abstract).
- Sinton,J.M. and Fryer,P. (1987) Mariana trough lavas from 18°N: implications for the origin of back arc basin basalts. *Jour.Geophys.Res.*,92,12782-12802.
- Stolper,E. (1980) A phase diagram for mid-ocean ridge basalts: Preliminary results and implications for petrogenesis. *Contrib.Mineral.Petrol.*,74,13-27.
- Syedín,V.T. (1988) Features of Cenozoic basaltoid magmatism and the origin of the Japan Sea. *J.Phys.Earth*,36,S107-S115.
- Sugimura,A., Matsuda,T., Chinzei,K., and Nakamura,K. (1963) Quantitative distribution of late Cenozoic volcanic materials in Japan. *Bull.Volcanol.*,26,125-140.
- Tada,R. (1990) Evolution of sedimentary environment in Japan Sea since the initiation of Yamato Basin. *Geol.Soc.Japan*,1990 meeting (Abstract in Japanese).
- Takahashi,E. (1978) Partitioning of Ni^{2+} , Co^{2+} , Fe^{2+} , Mn^{2+} , and Mg^{2+} between olivine and silicate melts: compositional dependence of partition coefficient. *Geochim.Cosmochim.Acta*,42,1829-1844.
- Takahashi,E. (1986) Origin of basaltic magma - Implication from peridotite melting experiments and an olivine fractionation model. *Bull.Volcanol.Soc.Japan*, S17-S40 (in Japanese with English abstract).
- Takahashi,E. and Kushiro,I.(1983) Melting of dry peridotite at high pressure and basalt magma genesis. *Amer.Mineral.*, 68, 859-879.

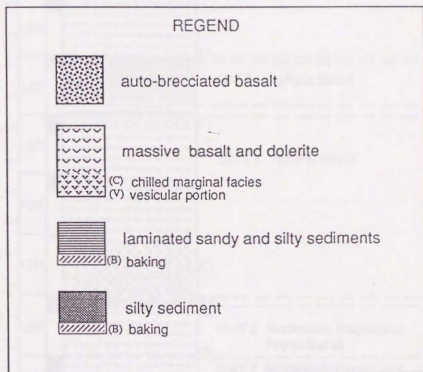
- Takimoto, T. (1986) Miocene volcanic rocks from the eastern part of the Shimokita peninsula, Northeast Japan - with special reference to the primitive tholeiite - . J. Japan.Assoc.Mineral. Petrol. Econ. Geol.,81,93-104 (Japanese with English abstract).
- Tamaki,K. (1985) Two modes of back-arc spreading. *Geology*,13,475-478.
- Tamaki,K. (1988) Geological structure of the Japan Sea and its tectonic implications. *Bull.Geol.Surv.Japan*,39,269-365.
- Tamaki,K., Pisciotto,K., Allan,J. et al. (1990) *Proc.ODP,Init.Repts.,127*. College Station, TX (Ocean Drilling Program).
- Tatsumi,Y., Sakuyama,M., Fukuyama,H., and Kushiro,I. (1983) Generation of arc basalt magmas and thermal structure of the mantle wedge in subduction zones. *J.Geophys.Res.*,88,5815-5825.
- Tatsumi,Y. (1986) Formation of the volcanic front in subduction zones. *Geophys.Res.Lett.*,13,717-720.
- Tatsumi,Y., Hamilton,D.L., and Nesbitt,R.W. (1986) Chemical characteristics of fluid phase released from a subducted lithosphere and origin of arc magmas: evidence from high-pressure experiments and natural rocks. *J.Volcanol.Geochem.Res.*,29,293-309.
- Tatsumi,Y., Nohda,S., and Ishizaka,K. (1988) Secular variation of magma source compositions beneath the northeastern Japan arc. *Chemical Geol.*,68.,309-316.
- Tatsumi,Y.,Otofuji,Y, Matsuda,T., and Nohda,S. (1989) Opening of the Japan Sea back-arc basin by asthenospheric injection. *Tectonophys.*
- Thompson,R.N. (1974a) Primary basalts and magma genesis. I. Skye, North-West Scotland. *Contrib.Mineral.Petrol.*,45,317-341.

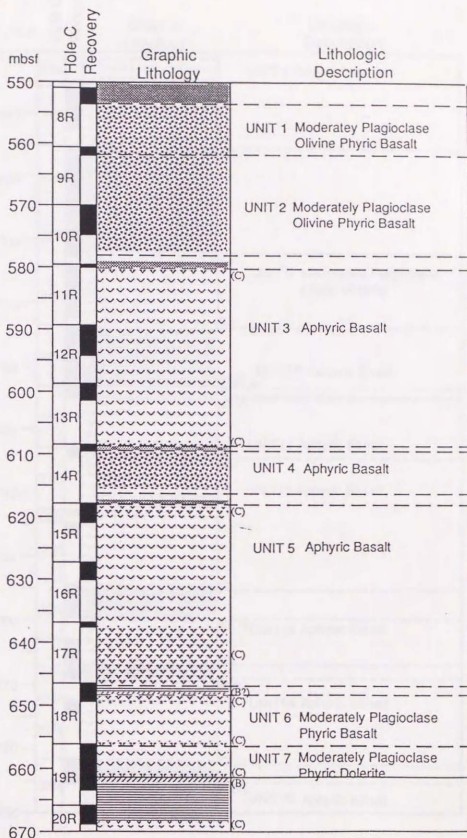
- Thompson, R.N. (1974b) Some high-pressure pyroxenes. *Mineral Magazine.*, 39, 768-787.
- Thompson, R.N. and Kushiro, I. (1972) The oxygen fugacity within graphite capsules in piston cylinder apparatus at high pressures. *Carnegie Inst. Washington, Yearb.*, 71, 615-616.
- Tokuyama, H., Suyemasu, M., Tamaki, K., Nishiyama, E., Kuramoto, S., Suyehiro, K., Kinoshita, H., and Taira, A. (1987) Report on DELP 1985 Cruise in the Japan Sea. Part III: Seismic reflection studies in the Yamato basin and the Yamato rise area. *Bull. Earthq. Res. Inst. Univ. Tokyo*, 62, 367-390.
- Tosha, T. and Hamano, Y. (1988) Paleomagnetism of Tertiary rocks from the Oga Peninsula and the rotation of northeast Japan. *Tectonics*, 7, 653-662.
- Tsuchiya, N. (1989) Submarine basalt volcanism of Miocene Aosawa Formation in the Akita-Yamagata oil field basin, back arc region of northeast Japan. *Memoir. Geol. Soc. Japan.*, 32, 394-408.
- Tsunakawa H., Takeuchi, A. and Amano, K. (1983) K-Ar ages of dykes in northeast Japan. *Geochemical Jour.*, 17, 269-275.
- Ui, T. (1979) Temporal and spatial distribution of Neogene volcanoes. In: Kammerer, K., Hashimoto, M., and Matsuda, T. (editors). *Geology of Japan*. Iwanami, Tokyo, 217-249p (in Japanese).
- Ulmer, P. (1989) The dependence of the Fe^{2+} - Mg cation-partitioning between olivine and basaltic liquid on pressure, temperature, and composition. An experimental study to 30 kbars. *Contrib. Miner. Petrol.*, 101, 261-273.
- Uto, K., Shibata, K., and Uchiumi, S. (1989) K-Ar ages of Neogene volcanic rocks from Northeast Japan: 1. the Mitaki and the Takadate Formations from Sendai district, Miyagi Prefecture. *J. Geol. Soc. Japan*, 95, 865-872 (in Japanese with English abstract).

- Verhoogen, J. (1973) Possible temperatures in the oceanic upper mantle and the formation of magmas. *Geol.Sci.Amer.Bull.*, 84, 515-522.
- Walker, D., Shibata, T., and DeLong, S.E. (1979) Abyssal tholeiites from the Oceanographer fracture zone. II. Phase equilibria and mixing. *Contrib.Mineral.Petrol.*, 70, 111-125.
- Weaver, S.D., Saunders, A.D., Pankhurst, R.J., and Tarney, J. A geochemical study of magmatism associated with initial stages of back-arc spreading. *Contrib.Mineral.Petrol.*, 68, 151-169.
- Yamaji, A. (1990) Rapid intra-arc rifting in Miocene Northeast Japan. *Tectonics*, 9, 365-378.
- Yamaji, A. and Sato, H. (1989) Miocene subsidence of the Northeast Honshu arc and its mechanism. *Memoir.Geol.Soc.Japan*, 32, 339-349 (Japanese with English abstract).
- Yamashita, S. (1988a) Petrogenesis of volcanic rocks dredged from the Meiyō Daini Seamount, Yamato Basin, Japan Sea. M.thesis, Chiba University.
- Yamashita, S. (1988b) Petrological characteristics of volcanic rocks from seamounts in Yamato Basin. *Marine Sci.Month.*, 11, 664-669 (in Japanese).
- Yoder, Jr., H.S. (1976) *Generation of basaltic magma*. National Academy of Sciences, Washington, D.C., 12-43p.

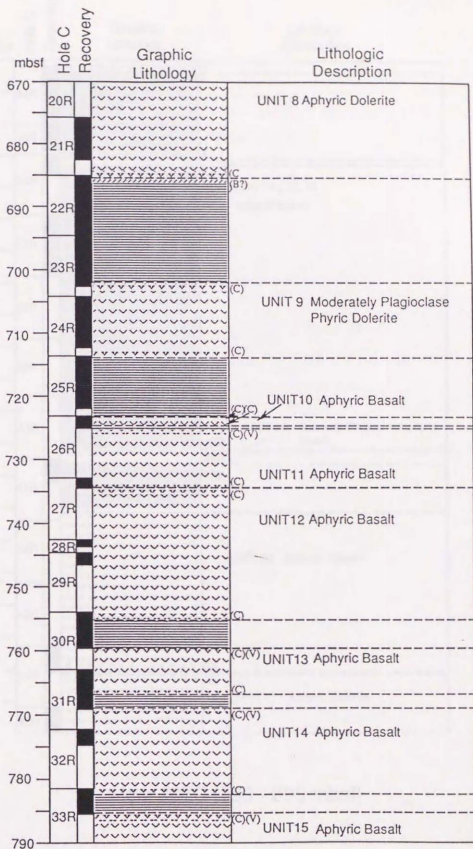
Appendix-A

Detailed lithostratigraphic columns of the basement of the Yamato basin cored during Ocean Drilling Program Leg 127/128. Locations of each hole are shown in Fig.2-2, Chapter 2. The columns followed after Tamaki, Pisciotto, Allan et al. (1990) except for that of Hole 794D which was described in Ingle, Suyehiro, von Breyman et al. (1990). The lithologic descriptions on the basaltic bodies are made by the manner newly defined in this study (see petrographic classification in §3-2).

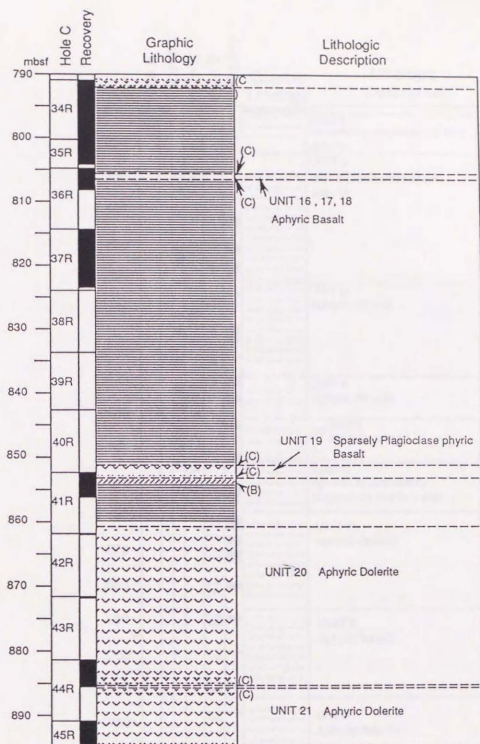




Hole 797C (550 - 670 mbsf)



Hole 797C (670 - 790 mbsf)



Hole 797C (790 - 895 mbsf)

Appendix-B

Whole rock major- and trace-element X-ray fluorescence analyses on the basement basaltic rocks from the Yamato basin. Stratigraphic positions of each measured samples are denoted by core# and the lithostratigraphic columns of the cored basement given in Appendix-A.

Each "UNIT" number denotes a single intrusive or effusive unit assigned on board during Ocean Drilling Program Leg 127/128 (see Appendix-A).

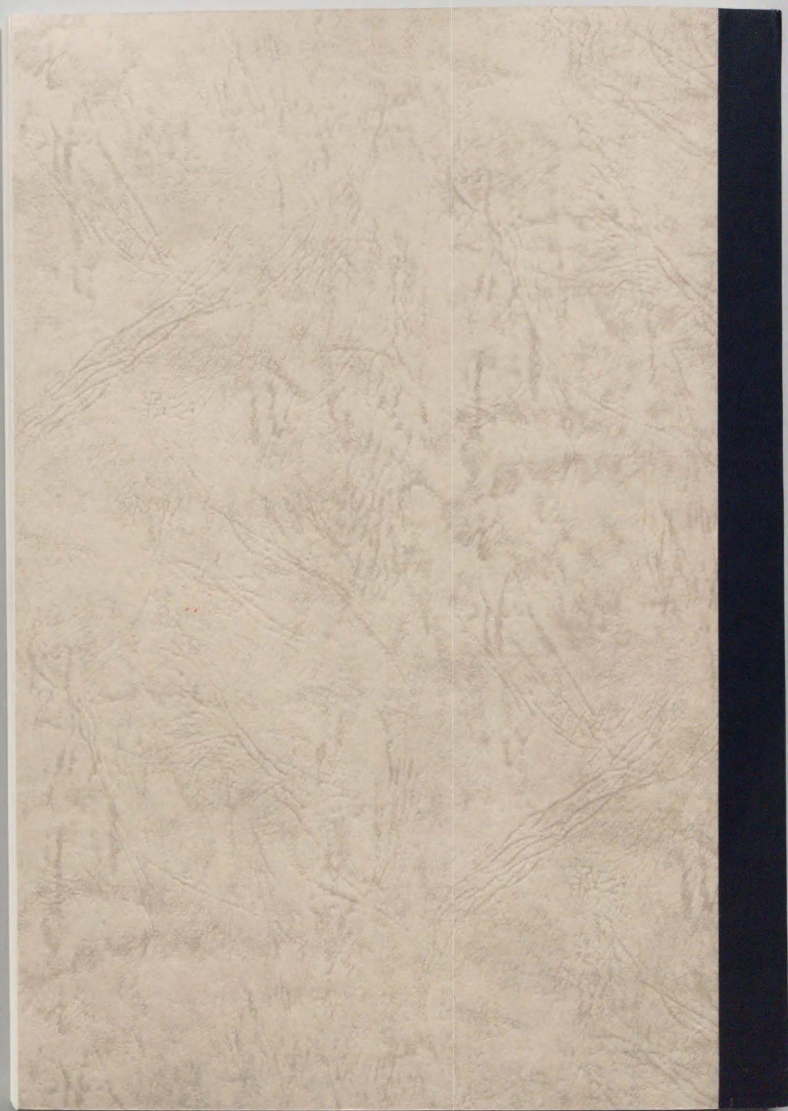
"Anal.ID"s denote the laboratories performed the XRF analyses: 127SB: Shipboard XRF analyses during ODP Leg 127 (Tamaki, Pisciotto, Allan et al., 1990); 128SB: Shipboard XRF analyses during ODP Leg 128 (Ingle, Suyehiro, von Breyman et al., 1990); ERI: XRF analyses at Earthquake Research Institute, University of Tokyo (this study). The analyses on the samples with the same core# were made on the strictly identical powder lot.

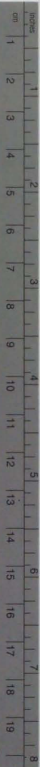
HOLE CORE#	797C 18R2770		797C 18R3160		797C 19R2742		797C 19R461		797C 20R2104		797C 21R1162		797C 24R6108		797C 26R1176		797C 26R261		797C 27R1130		
	UNIT	1275B	ERI	1275B	ERI	1275B	ERI	1275B	ERI	1275B	ERI	1275B	ERI	1275B	ERI	1275B	ERI	1275B	ERI	1275B	
SiO2	48.14	49.09	48.89	48.50	48.14	45.37	46.39	47.86	48.51	47.98	52.21	51.43	52.21	51.43	47.69	49.35					
TiO2	1.11	0.37	0.83	0.96	0.88	0.66	1.10	0.88	1.08	0.92	3.08	2.99	3.08	2.99	2.25	1.87					
Al2O3	19.32	17.43	17.97	17.90	17.97	20.69	20.53	18.06	17.02	17.40	13.01	15.03	15.03	17.93	17.93	15.91					
FeO	6.83	7.09	6.83	6.47	6.47	6.09	8.20	6.05	7.33	7.67	10.86	10.47	10.50	9.66	9.66	8.66					
MnO	4.34	4.27	4.33	4.22	4.22	4.74	4.25	4.19	4.19	4.25	4.28	4.28	4.28	4.28	4.28	4.20					
MgO	6.37	7.27	7.15	7.15	7.15	8.17	12.65	8.10	8.10	8.10	8.10	8.10	8.10	8.10	8.10	8.10					
CaO	10.02	11.47	11.44	11.64	11.67	10.45	12.60	10.30	11.54	11.55	3.80	3.84	3.84	3.84	3.84	3.84					
Na2O	3.46	3.02	3.36	2.91	3.09	3.55	2.81	3.40	2.82	2.80	4.18	4.48	4.48	4.48	4.48	4.48					
K2O	0.05	0.10	0.06	0.10	0.07	0.08	0.40	0.13	0.16	0.12	1.04	1.03	1.03	1.18	1.18	0.38					
PO2	0.12	0.08	0.09	0.08	0.08	0.09	0.10	0.09	0.10	0.10	0.43	0.43	0.43	0.32	0.32	0.25					
Total	97.88	97.02	98.19	97.45	97.63	97.53	97.23	97.44	97.70	98.12	98.49	98.84	97.54	96.99							
LOI	3.61	n.d.	2.82	n.d.	2.4	7.06	6.44	4.17	n.d.	2.12	n.d.	3.06	4.35	3.42							
Rb	n.d.	n.d.	n.d.	n.d.	n.d.	1	9	n.d.	n.d.	1	7	7	7	6	6	2					
Sr	237	217	215	174	179	189	138	189	221	218	302	305	302	191	298						
Ba	22	n.d.	2	n.d.	17	12	15	26	10	4	213	217	217	104	127						
Y	16	23	20	21	21	21	15	20	23	20	56	53	43	39	39						
Zr	80	58	54	50	54	62	67	61	71	67	298	283	211	162	162						
V	214	205	200	203	200	260	215	183	194	187	449	409	370	328	328						
Cr	284	352	309	357	317	396	314	272	330	293	37	14	178	169	169						
Ni	158	98	102	99	101	106	153	143	89	94	13	11	33	39	39						
Cu	85	85	84	84	83	86	76	67	67	73	24	39	62	62	62						
Zn	71	60	59	64	61	65	68	59	60	57	123	126	166	89	89						
Ga	16	n.d.	n.d.	14	n.d.	n.d.	n.d.	n.d.	1	2	1	2	11	8	6						
Nb	1	2	n.d.	3	n.d.	n.d.	n.d.	n.d.	1	2	1	12	11	8	6						
La	12	12	9	10	10	14	15	5	13	10	43	57	31	31	31						
Ce	13	9	10	2	9	14	31	31	31	31	37	37	37	37	37						
Sc	31	31	31	36	n.d.	n.d.	n.d.	n.d.	n.d.	n.d.	n.d.	n.d.	n.d.	n.d.	n.d.						
Th	2	2	n.d.	n.d.	n.d.	n.d.	n.d.	n.d.	n.d.	n.d.	n.d.	n.d.	n.d.	n.d.	n.d.						

HOLE CORE#	797C 28R1/49		797C 29R1/57		797C 29R1/69		797C 31R2/46		797C 31R2/56		797C 32R2/15		797C 34R1/33		797C 45R4/15		794B 26R2/01		794C 1R1/48	
	797C 28R1/49	797C 29R1/57	797C 29R1/69	797C 31R2/46	797C 31R2/56	797C 32R2/15	797C 34R1/33	797C 34R1/63	797C 34R1/33	797C 34R1/63	797C 34R1/33	797C 34R1/63	797C 34R1/33	797C 34R1/63	797C 45R4/15	797C 45R4/15	794B 26R2/01	794B 26R2/01	794C 1R1/48	794C 1R1/48
Anal/ID	ERI	1275B	ERI	1275B																
SiO2	53.65	52.53	54.28	52.31	52.31	50.87	50.24	49.72	49.16	52.10	49.49	49.52	51.67	49.93	50.82					
TiO2	2.27	2.18	1.90	2.02	1.78	1.65	1.78	1.95	1.75	2.00	1.94	1.85	1.49	1.38	1.37					
Al2O3	14.42	14.34	14.80	14.62	14.72	14.91	16.31	16.31	16.51	15.59	15.34	15.02	18.23	17.59	18.45					
FeO*	5.68	5.46	5.19	5.36	5.63	5.25	5.19	5.19	5.96	10.36	5.22	10.45	8.66	9.25	9.21					
MnO	0.17	0.18	0.14	0.18	0.16	0.19	0.27	0.31	0.31	0.49	0.40	0.19	0.09	0.16	0.17					
MgO	6.01	6.19	5.67	5.69	6.20	6.13	6.82	7.10	6.52	7.10	6.52	6.95	8.48	6.65	7.02					
CaO	5.32	5.27	6.16	6.53	10.04	10.04	8.79	8.78	1.35	9.23	3.44	3.69	3.47	6.76	6.63					
NiO	3.85	4.42	3.79	4.14	3.34	3.85	3.85	3.50	3.72	3.73	3.44	2.91	2.68	3.92	3.44					
K2O	0.18	1.17	0.10	0.59	0.22	0.32	0.50	0.54	0.46	0.35	0.26	0.26	0.58	0.26	0.26					
P2O5	0.32	0.32	0.31	0.33	0.33	0.33	0.32	0.34	0.24	0.35	0.26	0.26	0.30	0.24	0.24					
LOI	97.08	97.10	97.36	97.64	97.69	97.72	97.16	96.01	98.03	96.28	97.42	98.12	96.34	99.07	98.87					
LOI		2.53		2.08		1.64		2.54		4.37			4.32		2.23					
Rb	16	15	16	14	2	3	1	2	32	21	9	3	11	21	21					
Sr	269	265	274	275	283	276	337	329	110	303	276	276	257	352	349					
Ba	235	242	219	242	166	161	130	145	282	170	170	166	264	274	274					
Y	47	45	44	39	40	34	37	33	35	35	35	41	19	25	20					
Zr	247	231	233	207	169	160	171	159	224	183	168	103	100	97	100					
V	347	306	292	303	278	266	318	293	293	283	321	298	270	278	263					
Cr	29	11	45	26	140	134	229	196	85	151	158	33	59	40	40					
Mn	13	14	18	18	35	36	58	60	29	42	49	15	14	11	11					
Cu	27	46	30	45	49	59	64	69	42	49	48	48	22	71	77					
Zn	104	109	80	86	82	87	90	87	92	91	75	75	45	272	266					
Ga	21		20	20	20	20	20	20	20	20	20	20	20	20	20					
Nb	10	8	9	8	8	6	7	6	9	8	6	6	8	8	8					
La	10		22	14	14	14	19	19	32	44	14	11	11	12	12					
Ce	49	41	48	36	35	40	29	32	44	41	31	31	23	28	21					
Sc	28		31	24	24	24	39	39	36	36	36	29	2	3	3					
Th	5		4	3	3	3	1	1	3	3	3	2	2	1	1					

HOLE CORE#	794C		794C		794C		794C		794C		794C		794C		794C	
	2R104	2R177	3R1115	3R1222	4R142	4R216	1R196	3R389	7R146	8R165	9R1130	10R2102	1275B	1275B	1275B	1275B
UNIT	2	2	2	2	2	2	2	2	2	2	2	2	2	2	2	2
Anal.ID	ERI	ERI	ERI	ERI	ERI	ERI	ERI	ERI	ERI	ERI	ERI	ERI	1275B	1275B	1275B	1275B
SiO2	50.33	50.49	50.05	50.57	49.88	51.21	50.46	50.64	50.04	51.23	51.65	51.46	50.10			
TiO2	1.27	1.24	1.28	1.14	1.15	1.09	1.23	1.31	1.27	1.26	1.13	1.18	1.25			
Al2O3	18.77	18.44	19.18	21.18	18.70	20.23	19.08	19.56	18.11	17.80	17.70	17.86	16.58			
FeO*	8.10	8.12	7.80	8.02	7.69	7.81	7.53	7.83	10.24	10.01	7.83	8.08	8.73			
MnO	0.13	0.10	0.12	0.12	0.12	0.13	0.12	0.13	0.12	0.15	0.14	0.16	0.12			
MgO	5.68	5.61	5.69	5.45	5.78	5.98	5.64	6.40	6.57	9.81	9.81	11.46	11.32			
CaO	9.33	8.52	10.51	10.75	10.42	10.60	10.18	8.91	9.50	6.21	7.18	5.80	6.87			
Na2O	3.78	3.31	3.05	3.33	3.05	3.39	3.18	3.46	3.25	3.89	3.35	3.48	3.15			
K2O	0.68	0.70	0.68	0.65	0.63	0.60	0.74	0.61	0.62	0.82	0.73	0.67	0.75			
P2O5	0.30	0.24	0.21	0.20	0.22	0.22	0.22	0.20	0.21	0.20	0.20	0.19	0.22			
Total	99.85	97.64	98.52	101.31	97.64	101.26	98.38	101.47	99.70	99.50	99.27	100.34	99.09			
LOI	1.72	1.93	1.72	1.95	1.72	1.66	1.66	2.16	1.73	2.52	3.17	3.68	3.37			
Rb	7	7	7	6	6	7	8	6	7	10	11	7	8			
Sr	387	413	420	424	404	405	405	395	370	273	260	255	248			
Ba	162	168	175	138	129	141	135	166	122	154	166	154	159			
Y	21	23	21	15	21	18	22	20	20	18	18	17	18			
Zr	103	99	98	92	77	68	68	106	85	90	92	83	95			
V	243	252	254	236	225	212	241	272	238	309	259	297	253			
Cr	81	65	46	55	61	63	78	47	79	229	259	364	254			
Ni	15	15	15	16	17	17	17	12	21	100	132	165	133			
Cu	44	31	42	30	43	27	40	30	34	62	53	56	32			
Zn	75	71	68	60	65	66	70	28	49	69	67	71	72			
Ga	20	19	19	17	17	19	19	18	6	7	5	4	9			
In	8	8	8	6	6	7	7	7	7	5	5	4	9			
La	n.d.	n.d.	n.d.	5	5	7	7	7	7	26	26	16	21			
Ce	27	31	17	19	28	26	28	40	22	14	26	16	21			
Sc	31	23	22	26	26	26	28	28	28	14	26	16	21			
Th	31	1	n.d.	n.d.	n.d.	n.d.	n.d.	1	1	1	1	1	1			

HOLE CORE#	794D	794D	794D								
	12R3/124	13R1/181	13R1/122	14R1/181	16R1/107	17R1/107	18R1/144	18R1/144	19R1/111	20R1/11	20R1/20
UNIT	7	7	7	7	12R5B	12R5B	12R5B	12R5B	12R5B	9	9
AnalID	ERI	ERI	ERI	12R5B	12R5B	12R5B	12R5B	12R5B	12R5B	ERI	12R5B
SiO2	48.79	48.64	48.79	49.20	50.01	48.84	49.37	48.42	48.49	48.49	47.73
TiO2	1.65	1.51	1.54	1.64	1.53	1.54	1.57	1.51	1.48	1.48	1.48
Al2O3	15.74	15.04	16.07	15.11	20.11	17.56	17.80	17.30	16.63	16.63	16.65
FeO*	10.51	11.55	10.15	11.66	8.49	9.96	8.68	10.53	9.34	10.64	10.64
MnO	0.15	0.18	0.16	0.21	0.22	0.28	0.27	0.20	0.16	0.21	0.21
MgO	7.50	8.26	8.14	7.08	7.65	7.49	7.39	7.99	7.60	9.36	9.36
CaO	10.61	10.63	10.68	10.82	7.91	10.79	10.76	10.61	10.71	10.18	10.18
Na2O	3.03	2.83	2.94	3.17	3.34	2.65	3.02	2.91	2.78	2.82	2.82
K2O	0.19	0.24	0.21	0.24	0.45	0.21	0.22	0.20	0.16	0.22	0.22
P2O5	0.16	0.16	0.15	0.17	0.25	0.18	0.19	0.17	0.16	0.17	0.17
Total	98.33	99.04	98.83	99.28	100.06	99.49	99.37	99.85	97.53	99.46	99.46
LOI		0.76	1.25	4.57	2.65	2.26	2.44	2.16			
Rb	n.d.	3	n.d.	4	5	3	3	3	n.d.	2	2
Sr	204	184	207	191	263	181	200	185	195	173	173
Ba	36	21	43	11	56	10	6	12	19	53	53
Y	33	31	33	33	29	31	33	29	30	26	26
Zr	100	90	95	95	131	97	107	92	98	92	92
Y	254	245	236	284	278	255	281	232	226	234	234
Cr	269	324	295	311	329	283	319	312	309	291	291
Ni	85	129	119	117	113	108	124	137	135	124	124
Cu	53	63	56	63	55	61	74	60	51	56	56
Zn	82	85	80	91	108	77	83	81	79	53	53
Ga	20		19						17		
Nb	3	3	3	3	4	2	3	2	4	2	2
La	3		n.d.						10		10
Ce	4	19	20	27	33	24	31	22	10	10	12
Sc	30								26		26
Th	n.d.		n.d.						1		1





Kodak Color Control Patches

© Kodak, 2007 TM Kodak

Blue	Cyan	Green	Yellow	Red	Magenta	White	3Color	Black
1	2	3	4	5	6	7	8	9
10	11	12	13	14	15	16	17	18
19	20	21	22	23	24	25	26	27

Kodak Gray Scale



© Kodak, 2007 TM Kodak

A 1 2 3 4 5 6 **M** 8 9 10 11 12 13 14 15 **B** 17 18 19

